PHYSICAL REVIEW D **85,** 055023 (2012)

Probing neutralino dark matter in the MSSM and the NMSSM with directional detection

D. Albornoz Vásquez,[1,2] G. Bélanger,[1] J. Billard,[3] and F. Mayet[3]

[1]*LAPTH, U. de Savoie, CNRS, BP 110, 74941 Annecy-Le-Vieux, France*

[2]*Institut d'Astrophysique de Paris, UMR 7095 CNRS, Université Pierre et Marie Curie, 98 bis Boulevard Arago, Paris 75014, France*

[3]*Laboratoire de Physique Subatomique et de Cosmologie, Université Joseph Fourier Grenoble 1, CNRS/IN2P3, Institut Polytechnique de Grenoble, Grenoble, France*

(Received 30 January 2012; published 28 March 2012)

We investigate the capability of directional detectors to probe neutralino dark matter in the minimal supersymmetric standard model and the next-to-minimal supersymmetric standard model with parameters defined at the weak scale. We show that directional detectors such as the future MIMAC detector will probe spin-dependent dark matter scattering on nucleons that are beyond the reach of current spin-independent detectors. The complementarity between indirect searches, in particular, using gamma rays from dwarf spheroidal galaxies, spin-dependent and spin-independent direct search techniques is emphasized. We comment on the impact of the negative results on squark searches at the LHC. Finally, we investigate how the fundamental parameters of the models can be constrained in the event of a dark matter signal.

DOI: 10.1103/PhysRevD.85.055023 PACS numbers: 95.35.+d, 14.80.Ly

I. INTRODUCTION

The existence of cold dark matter (DM) is inferred from a large number of astrophysical observations at various scales. Locally, the large discrepancy between Newton's law of gravitation and the observed rotation curves indicates that spiral galaxies should be embedded in a DM halo [1,2].

Candidates for this class of to-be-discovered particles naturally arise from extensions of the standard model of particle physics (e.g., supersymmetry), as long as an *ad-hoc* discrete symmetry is invoked to preserve the proton stability. Indeed, the lightest particle of the secluded sector [in supersymmetry: the lightest supersymmetric particle (LSP)] becomes stable and can be a good candidate for the cold DM present in the Universe especially if it is a weakly interacting massive particle (WIMP). Numerous DM candidates have been proposed in extensions of the standard model and include fermions, scalars or gauge bosons [3].

Tremendous experimental efforts on a host of techniques have been made in the field of WIMP detection, the main experimental issue being the WIMP-background discrimination. Directional detection of galactic DM has been proposed as a powerful tool to identify genuine WIMP events as such [4]. Recent studies have shown that, within the framework of dedicated statistical data analysis, a low-exposure directional detector could lead either to a high significance discovery of galactic DM [5–7] or to a conclusive exclusion [8], depending on the value of the unknown WIMP-nucleon cross section. In the case of a high significance detection, it would also be possible to go further and to constrain the WIMP properties, both from particle physics (mass, cross section) and galactic halo (velocity dispersions), within the framework of a model-independent analysis [9]. To achieve this would require a rather high spin-dependent (SD) cross section (of the order of 10^{-4} pb) and a low WIMP mass, comparable to the target nucleus mass, as a matter of fact below the electroweak scale. Most projects of directional detection [10] are low-pressure time projection chambers (50–100 mbar). It follows that there is an obvious size limitation, which in turn implies that directional detectors cannot scale up to ton-scale experiment as most of the current direct detection projects [11–23]. Then, to be competitive and complementary with planned and existing direct detectors, directional detection should focus on SD interaction for which a large fraction of the parameter space could be probed by planned directional experiments (see Sec. II).

DM models which can best be probed by directional SD detection are the ones with Majorana particles such as the neutralino in the minimal supersymmetric standard model (MSSM) or its extensions. Not only can the neutralino be light (below 100 GeV) but also its Majorana nature implies that different processes contribute to the SD or spin-independent (SI) interaction, namely, the Z exchange contributes only to the SD cross section. Both types of detection modes are therefore complementary. Vector DM candidates can also lead to a signal in the SD mode which is not directly correlated with the SI mode. However in most models studied previously [for example, Universal Extra-Dimensions (UED) or little Higgs [24,25]] the DM tends to be heavier than 100 GeV (even heavier than 1 TeV in the minimal UED case [26]) making it difficult to extract the DM properties for direct detection. Models with Dirac fermion DM get a contribution from Z exchange for both SI and SD, these DM candidates are therefore best probed by SI where one can take advantage of the coherence effect.

We will therefore consider only models with a Majorana DM particle, more specifically the neutralino in the MSSM

and in one of its extensions, the next-to-minimal supersymmetric standard model (NMSSM) [27]. The parameter space of these models consistent with collider physics, precision measurements, DM relic density as well as DM direct searches were examined in several studies assuming either some GUT-scale relations among the fundamental parameters [28–36] or the more general case of parameters defined at the electroweak scale [37–42]. The potential of indirect detection for probing these models was examined, for example, in [43–49] and the complementarity between detection techniques were investigated in [50–53]. In particular, in a previous study [54,55] the allowed parameter space of the MSSM and of the NMSSM with light neutralinos (up to 50 GeV) was explored using a Markov Chain Monte-Carlo (MCMC) approach. Furthermore indirect detection of DM through the flux of photons from dwarf spheroidal galaxies, as well as direct detection limits from XENON100 were shown to be complementary and to further constrain the parameter space.

In this study we first determine the parameter space of the MSSM and NMSSM that can be explored by directional SD interactions with the future MIMAC detector [56]. For this we consider in both models the whole spectrum of masses for neutralinos although we use a restricted set of free parameters at the electroweak scale. We then compare this with limits from SI and indirect detection searches, namely, gamma rays. Finally, we investigate how the fundamental parameters of the models can be constrained in the event of a DM signal.

The paper is organized as follows. In Sec. II we discuss the potential of SD directional detector in probing DM. In Sec. III we discuss the expectation for the SD cross section. The parameter space of the model considered and the scanning method used are presented in Sec. IV. Our results for the SI/SD direct searches as well as for the flux of photons relevant for indirect searches are presented in Sec. V highlighting the complementarity between different techniques. The impact of directional detectors on probing the parameter space of the model is also addressed while the impact of the LHC on these results is sketched in Sec. VI. An investigation on how the observation of a signal could be used to determine some parameters of the supersymmetric model is carried out in Sec. VII.

II. DIRECTIONAL DETECTION FRAMEWORK

A. Directional detectors

There is a worldwide effort toward the development of a large time projection chamber devoted to directional detection [10] and all current projects [56–61] face common experimental challenges and share a unique goal: the simultaneous measurement of the energy (E_r) and the direction of the 3D track (Ω_r) of low-energy recoils, thus allowing the evaluation of the double-differential spectrum $d^2R/dE_r d\Omega_r$ down to the energy threshold. It is worth emphasizing that it is the lowest energy at which both the track and the energy can be retrieved which is the key experimental issue for directional detection. It follows that, to maximize the track length, the pressure of the gaseous detector must be as low as possible, leading to rather small detector masses as the volume cannot be arbitrarily large. One may then come to the conclusion that the directional detection strategy should focus on SD interactions to be competitive with planned and existing direct detectors [11–23].

Then, the ideal directional target is a nucleus with nonvanishing spin. Leading candidates include: ^{1}H, ^{3}He and ^{19}F which has been early suggested as a golden target for SD DM searches [62]. CF_4 is indeed planned as a sensitive medium for most upcoming directional detectors [10].

In the following, as a working example, we present the case for a low exposure (30 kg · year) CF_4 time projection chamber, operated at low pressure and allowing 3D track reconstruction, with sense recognition down to 5 keV. Such performance is taken as the ultimate limit for a directional detector. A complete overview of the effect of the main experimental issues of directional detectors, such as background contamination, energy threshold, sense recognition efficiency, angular and energy resolution on exclusion limits and discovery potential, is presented in [6,8].

B. Directional detection

1. Directional event rate and astrophysical inputs

Directional detection depends crucially on the local WIMP velocity distribution [63–65]. The isothermal sphere halo model is often considered but it is worth going beyond this standard paradigm when trying to account for all astrophysical uncertainties. The multivariate Gaussian WIMP velocity distribution corresponds to the generalization of the standard isothermal sphere with a density profile $\rho(r) \propto 1/r^2$, leading to a smooth WIMP velocity distribution, a flat rotation curve and no substructure. The WIMP velocity distribution in the laboratory frame is given by

$$f(\vec{v}) = \frac{1}{(8\pi^3 \det \boldsymbol{\sigma}_v^2)^{1/2}} \exp\left[-\frac{1}{2} (\vec{v} - \vec{v}_\odot)^T \boldsymbol{\sigma}_v^{-2} (\vec{v} - \vec{v}_\odot) \right], \tag{1}$$

where $\boldsymbol{\sigma}_v = \mathrm{diag}[\sigma_x, \sigma_y, \sigma_z]$ is the velocity dispersion tensor assumed to be diagonal in the Galactic rest frame $(\hat{x}, \hat{y}, \hat{z})$ and $\vec{v}_\odot$ is the Sun's velocity vector with respect to the Galactic rest frame. When neglecting the Sun's peculiar velocity and the Earth's orbital velocity about the Sun, $\vec{v}_\odot$ corresponds to the detector velocity in the Galactic rest frame and is taken to be $v_\odot = 220\ \mathrm{km \cdot s^{-1}}$ along the $\hat{y}$ axis pointing toward the constellation Cygnus at ($\ell_\odot = 90°$, $b_\odot = 0°$), where ℓ and b are the Galactic latitude and longitude. This way, we can consider the three velocity dispersions along the three axis as nuisance parameters in order to take into account the effect of anisotropic WIMP velocity distribution when deriving the discovery potential

of upcoming directional detectors. The anisotropy is defined by the β parameter as

$$\beta = 1 - \frac{\sigma_y^2 + \sigma_z^2}{2\sigma_x^2}. \quad (2)$$

Hence, $\beta = 0$ corresponds to an isotropic WIMP velocity distribution while $\beta < 0$ corresponds to a tangential anisotropy and $\beta > 0$ to a radial anisotropy. Using the parametrization of the three velocity dispersions used in this study (see Table I), we are considering WIMP velocity distributions with $\beta = 0 \pm 0.25$ (68% C.L.). This range is compatible with recent results from N-body simulations which found $\beta = 0$–0.4 [66] and observations which found a nonvanishing β parameter in the solar neighborhood [67,68].

The directional recoil rate is given by [69]

$$\frac{d^2R}{dE_r d\Omega_r} = \frac{\rho_0 \sigma_0}{4\pi m_\chi m_r^2} F^2(E_r) \hat{f}(v_{\min}, \hat{q}), \quad (3)$$

with m_χ the WIMP mass, m_r the WIMP-nucleus reduced mass, ρ_0 the local DM density, σ_0 the WIMP-nucleus elastic scattering cross section, $F(E_r)$ the form factor (using the axial expression from [70]), $v_{\min}$ the minimal WIMP velocity required to produce a nuclear recoil of energy E_r and $\hat{q}$ the direction of the recoil momentum. Finally, $\hat{f}(v_{\min}, \hat{q})$ is the three-dimensional Radon transform of the WIMP velocity distribution $f(\vec{v})$; see [69] for more details.

As one can see from Eq. (3), the directional rate is directly proportional to the local DM density at Solar radius (ρ_0) which is also subject to important uncertainties. Following [6] we consider ρ_0 as a nuisance parameter, using $\rho_0 = 0.3 \pm 0.1$ GeV/cm^3. We used a mean value of 0.3 GeV/cm^3 for the sake of comparison between the different direct searches experiments.

The last astrophysical uncertainties to be considered when deriving the discovery potential of upcoming directional detectors is the velocity of the Solar System orbit's in the Galactic rest frame taken as $v_\odot = 220 \pm 30$ km/s.

It is worth noticing that other astrophysical uncertainties like the escape velocity could be taken into account when assessing the sensitivity of a given direct detection experiment. However, the escape velocity is not considered in this study as we are dealing with a low-mass target material (^{19}F) associated to a low-energy threshold. Indeed, as the minimal speed required to produce a 5 keV recoil energy is about $v_{\min} = 130$ km/s for a WIMP mass of 100 GeV/c^2, while the mean WIMP velocity in an earth-based detector is about 300 km/s, we can deduce that the effect of a finite escape velocity will be negligible.

As a conclusion, accounting for uncertainties on the astrophysical parameters is a step beyond the "standard DM model," i.e.. isotropic isothermal DM halo, with fixed values of density and Sun's circular velocity (see also [109–115]). Evaluating the properties of the DM halo is indeed still a subject of debates. The numerical values and uncertainties corresponding to these astrophysical inputs are given in Table I (see [6] for a detailed discussion).

TABLE I. Gaussian parametrization (mean and standard deviation) of the different astrophysical nuisance parameters.

Nuisance parameters	Gaussian parametrization
ρ_0 [GeV/c^2/cm^3]	0.3 ± 0.1
$v_\odot$ [km/s]	220 ± 30
σ_x [km/s]	$220/\sqrt{2} \pm 20$
σ_y [km/s]	$220/\sqrt{2} \pm 20$
σ_z [km/s]	$220/\sqrt{2} \pm 20$

2. Dark matter properties inferred from directional detection

As highlighted by several recent studies [5,7–9], directional detection may be a powerful tool to discriminate between the DM signal and the background one. Indeed, the correlation between the main incoming direction of the recoiling events in galactic coordinates with the Solar System's orbit around the Galactic Center has been shown to be a strong and convincing proof in favor of a DM detection. This kind of discrimination is even more relevant when considering the recent results from DAMA, CoGeNT and CRESST experiments which have observed candidate events whose origins are difficult to assess without directional information.

At first, one may think of using directional detection to set exclusion limits. Several methods have been proposed [8,71]. Figure 1 presents the expected rejection limit for a 30 kg · year CF_4 directional detector, in the background-free case [8] for which a standard limit has been derived using the classical Poisson statistics associated to a 0 observed event. It allows us to reach $\sim 10^{-6}$ pb, noticing that for highly background-contaminated data (~ 10 kg^{-1} · year^{-1}) the result would be about an order of magnitude higher.

However, directional detection may be used to go beyond the standard exclusion limit strategy. Indeed, it may allow us to discover DM [5,7], the proof of discovery being the fact that the signal points to the direction of the constellation Cygnus (to which the solar system's velocity vector is pointing). Hence, the goal is to identify a genuine WIMP signal as such. Using a frequentist profile likelihood ratio test statistics, and taking into account astrophysical and experimental uncertainties, one can determine the sensitivity of a given directional experiment [6]. It is defined, in our case, as the minimal cross section required to obtain a DM detection with a significance greater than the 3σ level ain 90% of the experiments. The expected sensitivity of a directional detector filled with CF_4 with a low exposure (30 kg · year) and a 5 keV energy threshold is displayed in Fig. 1. Such a directional detector should be able to reach a sensitivity down to a SD cross section of 10^{-5} pb for a WIMP mass of 20 GeV/c^2. As one can see

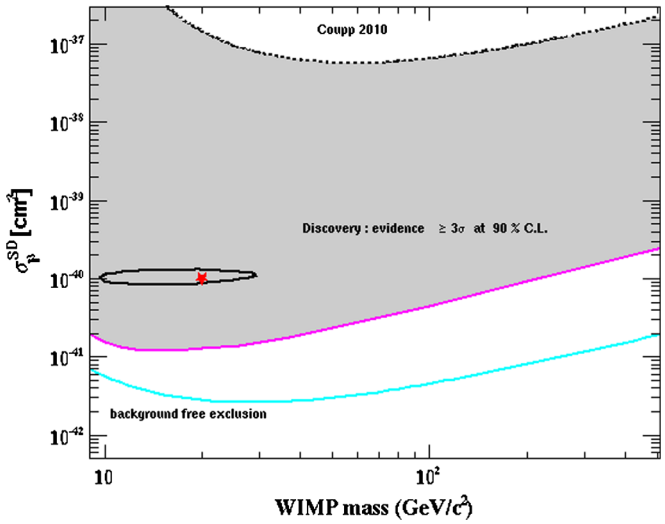

FIG. 1 (color online). Spin-dependent cross section on proton (cm^2) as a function of the WIMP mass (GeV) in the case of the pure-proton approximation [75] showing the sensitivity of a forthcoming 30 kg · year directional experiment (solid red line). It is defined as the minimal cross section required to obtain a DM discovery with a significance greater than the 3σ level at 90% C.L. [6]. For the same exposure, the dotted black line presents the projected exclusion limit [8] in the background-free case. The red star is the input value of the benchmark model and the black contour is the 68% contour level obtained with the MCMC analysis [9]. The exclusion limit from COUPP-2010 [11] (black dotted line) is also presented.

from the pink and cyan curves in Fig. 1, the distance between the background-free exclusion limit and the discovery sensitivity is lower at low WIMP mass than at high WIMP mass. This effect highlights the fact that directional detection is more sensitive to low WIMP mass as fewer events are required to reach a high significance detection for light WIMPs than for heavy WIMPs. This is of a major interest when considering the low-WIMP-mass issue as directional detection could bring valuable information to discriminate between a genuine WIMP detection and an unexpected background contamination of the DAMA, CoGent and CRESST experiments.

For high WIMP-nucleon SD cross sections, it is also possible to go even further [9]. With the help of a high-dimensional mutivariate analysis, it is possible to identify a WIMP with directional detection. It has been shown that dedicated analyses of simulated pseudodata of a 30 kg · year CF_4 directional detector would allow to constrain the WIMP properties, both from particle physics (m_χ, $\sigma_p^{\rm SD}$) and galactic halo (velocity dispersions). For instance, for a benchmark model ($m_\chi = 20$ GeV/c^2, $\sigma_p^{\rm SD} = 10^{-4}$ pb), the constraints would be the following

$$m_\chi = 19.9^{+2.7}_{-8.8}\ \text{GeV/c}^2 \qquad (68\%\ \text{C.L.}),$$
$$\log_{10}(\sigma_p) = -3.97 \pm 0.06 \qquad (68\%\,\text{C.L.}).$$

Figure 1 presents the 68% contour level in the (m_χ, σ_n) plane. This is indeed a model-independent measurement—as the velocity dispersions are set as free parameters within the framework of a multivariate Gaussian velocity distribution—of the WIMP properties, consistent with the input values and with a rather small dispersion.

To assess the interest of directional detection, either discovery or exclusion, in the following we explore the MSSM and NMSSM parameter space in order to check if some models, excluded neither by colliders nor cosmology, would lie in the regions of interest.

III. SPIN-DEPENDENT ELASTIC SCATTERING INTERACTIONS

A. Neutralino-nucleon spin-dependent cross section

In the nonrelativistic approximation, the WIMP-nucleon interaction is composed of two contributions: the spin-dependent (axial) and the spin-independent one (scalar) [72]. Two diagrams contribute to the SD interactions of a neutralino: the Z exchange and the squark exchange (see Fig. 2). The former relies on the Higgsino component of the LSP. When the Z contribution dominates, the amplitude for nucleon (a_N) is directly proportional to the neutralino Z coupling,

$$a_N = -(\Delta_u^N - \Delta_d^N - \Delta_s^N)(N_{13}^2 - N_{14}^2)$$

where N_{13}, N_{14} are the higgsino-d and higgsino-u components of the LSP and the coefficients Δ_q^N describe the contribution of a quark q to the spin of the nucleon. With

$$\Delta_u^p = 0.842 \pm 0.012 \qquad \Delta_d^p = -0.427 \pm 0.013$$
$$\Delta_s^p = -0.085 \pm 0.018$$

one can show [73] that the two amplitudes have opposite signs and that $a_p/a_n = -1.14 \pm 0.03$ independently of the parameters of the model. If the squark exchange is important, the relation between amplitudes are shifted and can even have the same sign. Note that the relative sign of a_p and a_n is a key point for SD direct searches as it could lead to either constructive or destructive interference between the two amplitudes, depending on the spin content of the considered nucleus target (see Sec. III B). The squark contribution to the amplitude reads

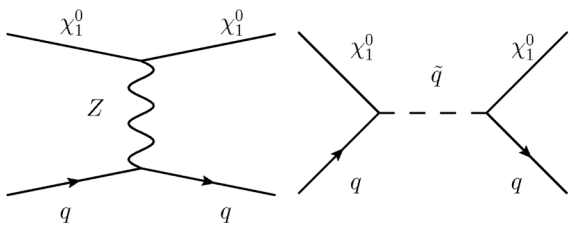

FIG. 2. Feynman diagrams contributing to spin-dependent elastic scattering of neutralinos on nucleons.

$$\frac{a_N}{8M_Z^2c_W^2} = \frac{t_W^2N_{11}^2}{9}\left(\frac{4\Delta_u^N}{m_{\tilde{u}_R}^2 - m_{\tilde{\chi}}^2} + \frac{\Delta_d^N + \Delta_s^N}{m_{\tilde{d}_R}^2 - m_{\tilde{\chi}}^2}\right) + \left(N_{12} + \frac{t_W}{6}N_{11}\right)^2 \frac{\Delta_u^N}{4(m_{\tilde{u}_L}^2 - m_{\tilde{\chi}}^2)} + \left(N_{12} - \frac{t_W}{6}N_{11}\right)^2 \frac{(\Delta_d^N + \Delta_s^N)}{4(m_{\tilde{d}_L}^2 - m_{\tilde{\chi}}^2)}, \quad (4)$$

where N_{11}, N_{12} are, respectively, the bino and wino component of the LSP, $c_W = \cos\theta_W$, and $t_W = \tan\theta_W$. In the limit of an almost pure bino LSP, which is usually the case for a light neutralino, the amplitude simplifies to

$$\frac{a_N}{8M_Z^2c_W^2} = \frac{t_W^2N_{11}^2}{9}\left[\frac{(\Delta_u^N + \Delta_d^N + \Delta_s^N)}{4(m_{\tilde{q}_L}^2 - m_{\tilde{\chi}}^2)} + \frac{4\Delta_u^N}{m_{\tilde{u}_R}^2 - m_{\tilde{\chi}}^2} + \frac{\Delta_d^N + \Delta_s^N}{m_{\tilde{d}_R}^2 - m_{\tilde{\chi}}^2}\right]. \quad (5)$$

If furthermore the L and R squark masses are equal, the dominant contribution comes from $\tilde{u}_R$ and $\tilde{d}_R$ respectively as the neutralino/quark/squark coupling is proportional to the quark hypercharge which is larger for RH quarks. The ratio of proton and neutron amplitudes is then $a_p/a_n = -3.38 \pm 0.22$. In the case where $\tilde{q}_L$ gives the largest contribution the ratio of amplitudes is positive with $a_p/a_n = 1$. The squark exchange is however usually suppressed as compared to the Z exchange because of the higher mass scale involved, $m_{\tilde{q}} \gg M_Z$. It can be dominant when the higgsino component is very small leading to a suppressed coupling of the neutralino to the Z and to small cross sections. In fact for the squark contribution to be relevant for the discovery reach of directional detection ($\sigma_p \simeq 5 \times 10^{-6}$ pb), one can estimate that the common squark mass has to be below roughly 620 GeV when the LSP is a light bino ($N_{11} = 1$). Such squark masses are excluded by LHC if the dominant decay mode of the squark is into q + LSP [74]. Note that a cancellation between the squark and Z exchange can lead to $\sigma_p \gg \sigma_n$ or $\sigma_p \ll \sigma_n$, we however stress that this occurs typically only for small cross sections if the squarks are near the TeV scale as will be discussed further in Sec. VI.

B. Constraining the spin-dependent cross section

The SD cross section (at zero momentum transfer) on a nucleus XA is given by

$$\sigma^{\mathrm{SD}}({}^A\mathrm{X}) = \frac{32}{\pi}G_F^2\mu_A^2\frac{J+1}{J}(a_p\langle S_p\rangle + a_n\langle S_n\rangle)^2 \quad (6)$$

where G_F is the Fermi constant, μ_A^2 is the WIMP-nucleus reduced mass, J the total nuclear spin and $\langle S_{p,n}\rangle = \langle N \mid S_{p,n} \mid N\rangle$ the neutron/proton spin content of the target nucleus. To be sensitive to the SD interaction, one may either choose a pure nonzero spin nucleus target (^{3}He, ^{19}F) or rely on the isotopic fraction of the chosen target. This way, scalar detection experiments may also impose constraints on SD interaction thanks to the small fraction of odd-A target nucleus in the sensitive medium (e.g., ^{73}Ge for Ge-based detectors or ^{129,131}Xe for Xenon-based ones).

The result of a DM experiment, either a discovery or an exclusion, implies a constraint on $\sigma^{\mathrm{SD}}({}^A\mathrm{X})$ which must then be converted to a constraint on σ_p, n for the sake of comparison between various DM experiments using different target nuclei. This is however not straightforward as the amplitude on both proton and neutron are involved in (6).

For simplicity, the pure-nucleon coupling approximation ($a_n = 0$ or $a_p = 0$) is often used. This method is however WIMP-model-dependent as there is no particular reason for one coupling to vanish, indeed this does not occur in the MSSM. A model-independent method has been proposed by D. R. Tovey *et al.* [75] to enable comparison amongst SD direct searches of DM. For a given WIMP mass, an exclusion limit on $\sigma^{\mathrm{SD}}({}^A\mathrm{X})$ is then translated into a constraint on σ_p and σ_n, as:

$$\left(\sqrt{\sigma_p} \pm \frac{\langle S_n\rangle}{\langle S_p\rangle}\sqrt{\sigma_n}\right)^2 < \sigma_p^{\mathrm{lim}}$$

where σ_p^{lim} is the limit on WIMP-proton cross section obtained in the pure proton approximation. The limit is expressed, for a given WIMP mass, in the nucleon cross section plane (σ_p, σ_n) and divided into two cases: ''constructive'' and ''destructive,'' whether the diffusion amplitude on proton and neutron add up coherently or not, taking into account the relative sign of $\langle S_p\rangle$ and $\langle S_n\rangle$. Hence, the exclusion in the $(\sigma_p, \sigma_n, m_\chi)$ space does not depend on a particular WIMP model.

As outlined in [76], setting a limit on the SD interaction requires us to neglect the SI one, which is not always justified. In particular, in the case of Fluorine, the SD rate can be dominant over the SI, but this has to be checked in each particular WIMP model.

1. Proton-based versus neutron-based detectors

The knowledge of the expectation values of the spin content of the proton and neutron within the nucleus ($\langle S_{p,n}\rangle = \langle N \mid S_{p,n} \mid N\rangle$) is a key issue for SD detection of DM. The WIMP couples mainly to the spin of the unpaired proton (e.g., ^{19}F) or to the one of the unpaired neutron (e.g., ^{3}He), leading to a contraint on either the proton or neutron diffusion amplitude (a_n, a_p). One may then distinguish *proton-based* (^{19}F, ^{23}Na, ^{27}Al, ^{35}Cl, ^{127}I) and *neutron-based* (^{3}He, ^{73}Ge, ^{129}Xe) SD experiments which shall present an obvious complementarity [77–79].

However in practice, the spin of the target nucleus is carried both by constituent neutrons and protons and the comparison between SD experiments is not straightforward.

Detailed nuclear-shell-model calculations have been developed and the accuracy of the $\langle S_p \rangle$ and $\langle S_n \rangle$ evaluation is assessed by comparing, within the same shell model, the predictions on the magnetic moment and the energy spectra for the nuclear lowest eigenstates with experimental values. We refer the reader to [80] for a comprehensive discussion on the subject. Several collaborations have published exclusion limits on SD WIMP-nucleon cross sections [11–18,23]. In the following, we use (see Fig. 1):

(i) for proton-based detector: COUPP-2010 [11], obtained with a 2-liter CF_3I Bubble Chamber, with a 28.1 kg · day effective exposure,

(ii) for neutron-based detector: XENON10 [12], obtained with 5.4 kg of fiducial liquid xenon, with a 136 kg · day effective exposure.

2. The case of ^{19}F

In the following we emphasize that some discrepancies remain on the spin content of ^{19}F. The value of the spin content of ^{19}F is predicted by two authors [81,82]; see Table II. It is dominated by the proton content but the neutron one varies by more than 1 order of magnitude. Values from A. F. Pacheco and D. Strottman are widely used. However, it is noteworthy that the evaluation from P. C. Divari *et al.* is obtained by shell-model calculations using the Wildenthal interaction [83], which is known to reproduce accurately many nuclear observables.

Nonetheless, to allow a fair comparison with existing published results [11,18], the values $\langle S_p \rangle = 0.441$ and $\langle S_n \rangle = -0.109$ from [82] are chosen, noticing that the other choice would only mildly alter the result on the proton cross section limit but would scale up the result for neutron cross section by 2 orders of magnitude (see. Figure 3). We leave the question open, highlighting the fact that results on ^{19}F must be treated with caution owing to the nuclear-shell-model dependence.

TABLE II. Spin content of ^{19}F in various nuclear-shell models. Henceforth, values from [82] are used.

Model	$\langle S_p \rangle$	$\langle S_n \rangle$	Ref.
odd-group	0.5	0.	
Pacheco and Strottman	0.441	−0.109	[82]
Divari *et al.*	0.475	−0.0087	[81]

However, it is worth emphasizing that, in the case of ^{19}F, the spin contents having opposite sign, one expects a constructive interference between the proton and neutron amplitudes, as they usually also have opposite sign (Sec. III A).

Figure 3 presents, for a 20 GeV WIMP, the sensitivity of the considered directional detector. The light grey area is the region already excluded by the most constraining experiments (COUPP-2010 [11] and XENON10 [12]). In the case of XENON10, the curve is derived from [12] considering a pure ^{129}Xe detector, which is justified as the contribution of odd xenon isotopes are very close. In the case of COUPP, the curve is derived from [11] considering a pure ^{19}F detector, i.e., neglecting the contribution of

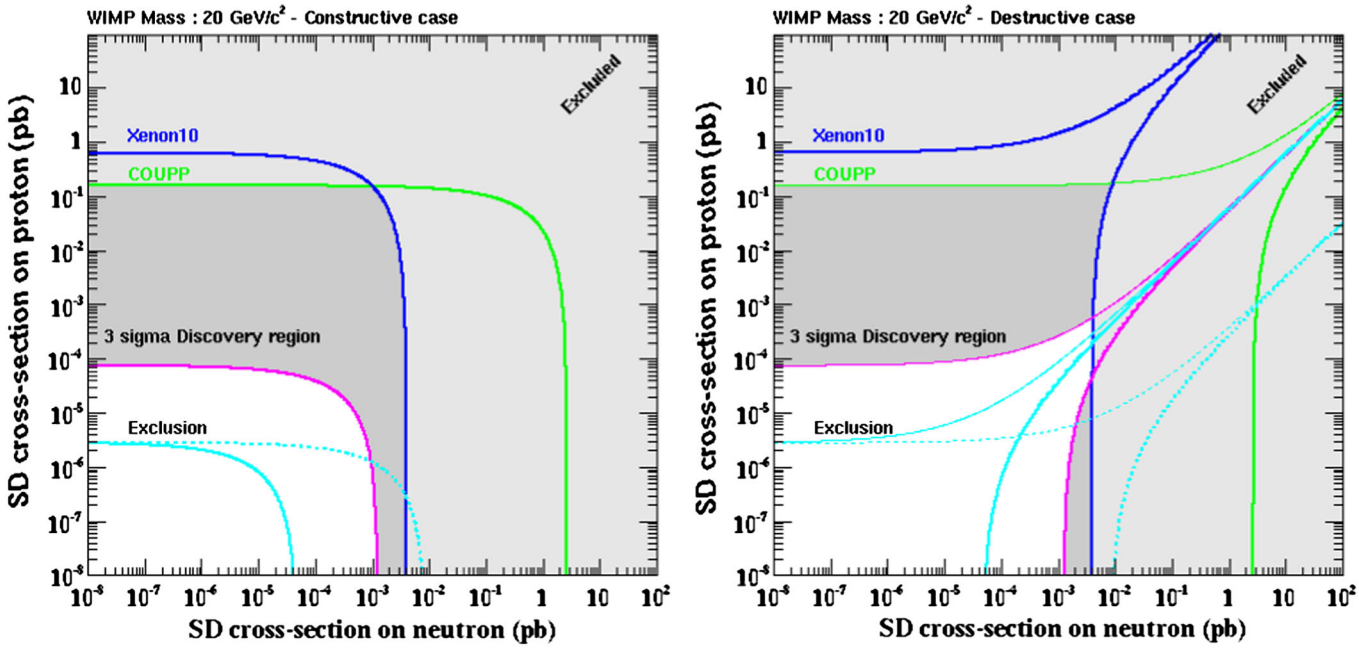

FIG. 3 (color online). Left (resp. right) panel present the constraints in the constructive (resp. destructive) case, for a 20 GeV. The light grey area is the region already excluded by the most constraining experiments (COUPP-2010 [11] and XENON10 [12]). For a 30 kg · year CF_4 directional detector, the dark grey area is the 3σ discovery region, while the solid light curve labeled "exclusion" is the background-free projected limit. Dashed light curve presents the same result for the alternative ^{19}F spin content values [81].

^{127}I for such a small WIMP mass. The exclusion limit and the 3σ discovery region, for a 30 kg · year CF_4 directional detector are presented on Fig. 3. It corresponds to a rather large region in the parameter space, well below current limits.

IV. TESTING SUPERSYMMETRIC CONFIGURATIONS

In order to establish the reach of directional detection for probing supersymmetric models, we take into account various constraints that have an impact on the parameter space.

A. Parameter space

We consider two models, both with parameters defined at the electroweak scale, the MSSM and the NMSSM. The free parameters we take in the MSSM are the same as in [55]. We assume minimal flavour violation, two common soft masses $M_{\tilde{l}_L}$ and $M_{\tilde{l}_R}$ for left-handed and right-handed sleptons, equality of the soft squark masses between the first and second generations, $M_{\tilde{q}_{1,2}}$, while the mass of the third-generation squarks is kept as an independent free parameter $M_{\tilde{q}_3}$. We allow for only one nonzero trilinear coupling, A_t. The gaugino masses M_1,M_2 and M_3 are free parameters as well. In particular this allows us to have $M_1 \ll M_2$, implying a light neutralino much below the EW scale [84–88]. The ratio of the doublet Higgs VEV' $\tan\beta$, is also a free parameter in both models. In the MSSM, the Higgs bilinear term, μ, and the pseudoscalar mass M_A are the remaining free parameters. Thus we consider MSSM scenarios with the 11 following free parameters[1]

$$M_1, M_2, M_3, \mu, \tan\beta, M_A, M_{\tilde{l}_L}, M_{\tilde{l}_R}, M_{\tilde{q}_{1,2}}, M_{\tilde{q}_3}, A_t.$$

The NMSSM is a simple extension of the MSSM with an additional gauge singlet superfield, S, that provides a solution to the naturalness problem. Indeed the parameter $\mu = \lambda\langle S\rangle$ is determined by the VEV of the scalar singlet and is thus naturally of the EW scale [27]. In the NMSSM there are additional parameters related to the extended Higgs sector. Note that we will use μ rather than $\langle S\rangle$ as a free parameter to remain close to the MSSM parametrization. The part of the superpotential involving Higgs fields reads

$$W = \lambda S H_u H_d + \frac{1}{3}\kappa S^3$$

and the soft Lagrangian is

$$\mathcal{L}_{\text{soft}} = m_{H_u}^2|H_u|^2 + m_{H_d}^2|H_d|^2 + m_S^2|S|^2 + \left(\lambda A_\lambda H_u H_d S + \frac{1}{3}\kappa A_\kappa S^3 + \text{H.c.}\right).$$

After using the minimization conditions of the Higgs potential, the Higgs sector, which consists of three neutral scalar fields, H_1, H_2, H_3 and two pseudoscalar neutral fields, A_1, A_2 as well as a charged Higgs, $H^\pm$ is described by six free parameters, μ, $\tan\beta$ as well as λ, κ, A_λ and A_κ. The list of free parameters therefore contains the ones of the MSSM with the pseudoscalar mass, M_A, replaced by

$$\lambda, \kappa, A_\lambda, A_\kappa,$$

for a total of 14 free parameters.

These simplified models reproduce the salient features of neutralino DM. Indeed, apart from the mass of the LSP, the most important parameters are the gaugino/higgsino content of the LSP, determined by μ and M_1, M_2, $\tan\beta$, as well as the mass of the Higgses which can enhance significantly neutralino annihilations. Sfermion exchange, and, in particular, slepton exchange, can also play a role for light neutralinos.

There are many similarities between the MSSM and the NMSSM, as will be seen in the following analysis. However one characteristic feature of the NMSSM is that the singlet fields, which mostly decouple from the SM fields, can be very light and yet escape LEP bounds [27]. Therefore it is much easier to have light neutralinos because they can annihilate into or through the exchange of light singlet Higgses [89].

B. Scanning method

In order to thoroughly scan the parameter space we used a MCMC code, first presented in [54]. The scanning procedure consists on a Metropolis-Hastings algorithm, and is based on MICROMEGAS 2.4 [90–92] for the computation of all observables. The supersymmetric spectra are calculated with SUSPECT [93] in the MSSM and with NMSSMTOOLS [94] in the NMSSM. The latter also provides collider constraints on the Higgs sector, on sparticles and on flavour observables.

Each point is generated by making a random step with a normal variation from the previous point in each dimension. Then, we compute its total prior $\mathcal{P}$, total likelihood $\mathcal{L}$ and total weight $\mathcal{Q} = \mathcal{P} \times \mathcal{L}$. It is kept with a probability $\text{Min}(1, \mathcal{Q}'/\mathcal{Q})$, where $\mathcal{Q}'$ is the total weight of the point being tested and $\mathcal{Q}$ is that of the source point. If the evaluated point is not kept, then a new point is generated from the last accepted point. Thus, the parameter space is scanned via a random walk by iterating this procedure.

The priors we impose are: a set of parameters has to lie within the boundaries of the parameter space given by Table III, while a physical solution of the spectrum calculator and a neutralino LSP are required. Regarding likelihoods, these are displayed in Table I of [54]. We include

[1]We do not perform a thorough exploration of the much studied CMSSM because it is only a particular case of the MSSM. Furthermore in that model the LSP mass is above 50 GeV because of the Large Electron-Positron Collider limit on charginos and the relation between the chargino and the neutralino masses. This leaves few possibilities for parameter determination.

TABLE III. Intervals of free parameters used for the MSSM and NMSSM scans (GeV units).

Parameter	Minimum	Maximum	Tolerance	Model
M_1	1	1000	3	both
M_2	100	2000	30	both
M_3	500	6500	10	both
μ	0.5	1000	0.1	both
$\tan\beta$	1	75	0.01	both
M_A	1	2000	4	MSSM
λ	0	0.75	0.1	NMSSM
κ	0	0.65	0.08	NMSSM
A_λ	-5000	5000	100	NMSSM
A_κ	-5000	5000	100	NMSSM
A_t	-3000	3000	100	both
$M_{\tilde{l}_R}$	70	2000	15	both
$M_{\tilde{l}_L}$	70	2000	15	both
$M_{\tilde{q}_{1,2}}$	300	2000	14	both
$M_{\tilde{q}3}$	300	2000	14	both

limits on B physics observables, on the anomalous magnetic moment of the muon $(g-2)_\mu$, on the Higgs and sparticles masses obtained from LEP and the corrections to the ρ parameter. In the MSSM, the limits on the Higgs mass were applied by making use of the SUSY-HIT [95] and the HIGGSBOUNDS packages [96,97] as in [55]. The HIGGSBOUNDS version used (3.1.3) include LEP and Tevatron results as well as first LHC results. However, more recent results from CMS presented in [98,99] were only included in the analysis *a posteriori*. Notice that we take the WMAP measurement on the DM relic density as a strict upper limit on the LSP relic density –obtained via the usual freeze-out mechanism–, however, we allow the neutralino to have a relic density as low as 10% of the measured value. Indeed, the LSP could be only a fraction of the dark component, the rest corresponding to other dark particles or to a modified theory of gravity. For more details see [54].

The scans we performed in this study were aimed at giving a general determination of the different configurations with neutralino masses at the weak scale and below. However, as it was shown in [54,55], it is difficult to find light ($\lesssim 30$ GeV) neutralinos with a random walk in both the MSSM and the NMSSM: the probability of falling in these regions that require fine-tuning is rather small. Indeed, in the MSSM, the neutralino LSP has to annihilate via the exchange of either rather light Higgs bosons, scenarios that are heavily constrained by the Tevatron experiments as well as by CMS, or light sleptons, particularly of staus with masses close to the LEP lower bound of 81.9 GeV [100]. In the case of the NMSSM, it has been shown in [54,101] that the neutralino can achieve light masses by annihilating via or into very light singletlike Higgs bosons.

TABLE IV. Basic characteristics of the scans of the MSSM and the NMSSM. The 1σ, 2σ and 3σ, columns represent the fraction of points satisfying $0.32 \times \mathcal{Q}_{\max} \leq \mathcal{Q}$, $0.05 \times \mathcal{Q}_{\max} \leq \mathcal{Q}$ and $0.003 \times \mathcal{Q}_{\max} \leq \mathcal{Q}$ respectively.

	Points	$\mathcal{Q}_{\max}$	1σ	2σ	3σ
MSSM	1208949	0.755	0.25	0.68	0.97
NMSSM	2092875	0.812	0.30	0.72	0.98

Hence we used two different techniques to trigger the chains that scanned the parameter spaces. On one hand we let part of the chains start randomly, i.e., look randomly for a starting point with $\mathcal{Q} \neq 0$. On the other hand we used the previous knowledge of fine-tuned regions explored in [54,55] to set fixed starting points for the rest of the chains, in order to force the random walk to yield at least a few points in such regions.

A summary of the characteristics of the runs we present is given in Table IV.

V. RESULTS

Before analyzing the predictions for SD interactions, we impose further constraints on the parameter space of the models found by the MCMC. We focus on astroparticle constraints, including XENON100 limits on SI interactions [20] as well as limits from Fermi-LAT observations of the photon flux from dwarf spheroidal companions (dSphs) [102].[2]

A. Dark matter searches constraints

Dark matter observables are computed for each point kept by the MCMC. This includes the direct detection cross sections: SI and SD neutralino-nucleon elastic scattering processes, for both protons and neutrons, and the γ-ray flux produced by neutralino annihilations at low velocities.

Notice that the actual observables are: $\sigma_{scat}\rho_\odot$ for direct detection, i.e., the elastic scattering cross section times the neutralino density at Earth, and $\sigma_{\rm ann}\rho^2_{\rm loc}$ for γ-ray indirect detection, i.e., the neutralino annihilation cross section times the local neutralino density squared (in the astrophysical object). Since we allow for the neutralino to represent only a fraction of the DM component, we scale the neutralino density by the same fraction in all astrophysical systems. Thus we define

[2]Here we do not show the impact of recent LHC limits on the MSSM Higgs sector, in particular, the LHCb and CMS combined results on the $B_s \to \mu\mu$ branching ratio and the CMS negative search for $H \to \tau\tau$ constraining the $\tan\beta$ vs M_A plane. For an account of such an analysis over the same MSSM data set presented here; see [103].

$$\xi = \mathrm{Min}\left(\frac{\Omega_{\chi_1^0} h^2}{\Omega_{\mathrm{WMAP}} h^2}, 1\right),$$

where $\Omega_{\mathrm{WMAP}} h^2 = 0.1097$ is the 1σ lower limit of the DM density as obtained by the WMAP 5-year analysis [104].

1. Spin-independent elastic scattering

Spin-independent interactions result from Higgs and/or squark exchanges. Because of the mass scales involved, it is generally the Higgs contribution that dominates, providing the LSP is some mixture of higgsino/gaugino. In the MSSM, both the light and heavy Higgses can contribute, in particular, the heavy Higgs contribution is enhanced at large values of $\tan\beta$. In the NMSSM, there is in addition a contribution from the singlet Higgs. When the lightest scalar is below 10 GeV one can have an enhancement of the cross section even if the LSP is weakly coupled to the scalar Higgs [101]. The SI interaction rates depend on the quark content of the nucleons. Indeed, the choice of quark coefficients in nucleons could vary the estimation by an order of magnitude. In MICROMEGAS the quark content of nucleons is parametrized by the $\sigma_{\pi N}$ and σ_0 terms [90]. Recent lattice QCD results point towards small strange quark contributions, hence to $\sigma_{\pi N} \simeq \sigma_0$ [105]. We take $\sigma_{\pi N} = 45$ MeV and $\sigma_0 = 40$ MeV.

The predictions for SI interactions in the MSSM and the NMSSM along with XENON100 [20] and CDMS-II [23] limits are displayed in Fig. 4. Color tagging in relation with detectability in directional detection will be discussed in Sec. V C. The XENON100 limit attain some of the configurations found in both models, thus constraining the parameter spaces. Nevertheless, most scenarios lie below the XENON100 sensitivity, and many are more than an order of magnitude away from it. This highlights the need for complementarity in DM search strategies.

While in general the point distribution is rather similar in both models, there are a few differences between the two panels. Those differences can best be understood by investigating the effect of the relic density constraint which depends on the model. In particular, neutralinos below 30 GeV in the NMSSM usually imply a light Higgs scalar or pseudoscalar to ensure the annihilation rate is large enough to obtain relic densities below the WMAP value. If the light Higgs is a scalar, then the SI cross section gets enhanced, as shown in [101,106], whereas a light pseudoscalar does not contribute to the SI cross section. This explains the larger range of predicted cross sections observed in the NMSSM with respect to the MSSM. In the latter, as discussed in [55], when the relic density is achieved through as-light-as-possible scalar Higgs exchanges, the lighter the neutralino, the wider the mass difference between neutralinos and Higgses, thus the larger the coupling between these must be. Hence the SI cross section tends to increase towards lighter neutralino masses, which corresponds to the top-left arm of the cloud in the top panel of Figs. 4 top panel. However, when the neutralino annihilations are driven by slepton exchanges, the SI cross section does not evolve with the neutralino mass, and is not necessarily enhanced by the need of large neutralino-Higgs couplings. That situation corresponds to the other light neutralino arm, a more diffuse cloud at smaller interaction rates, in the same panel.

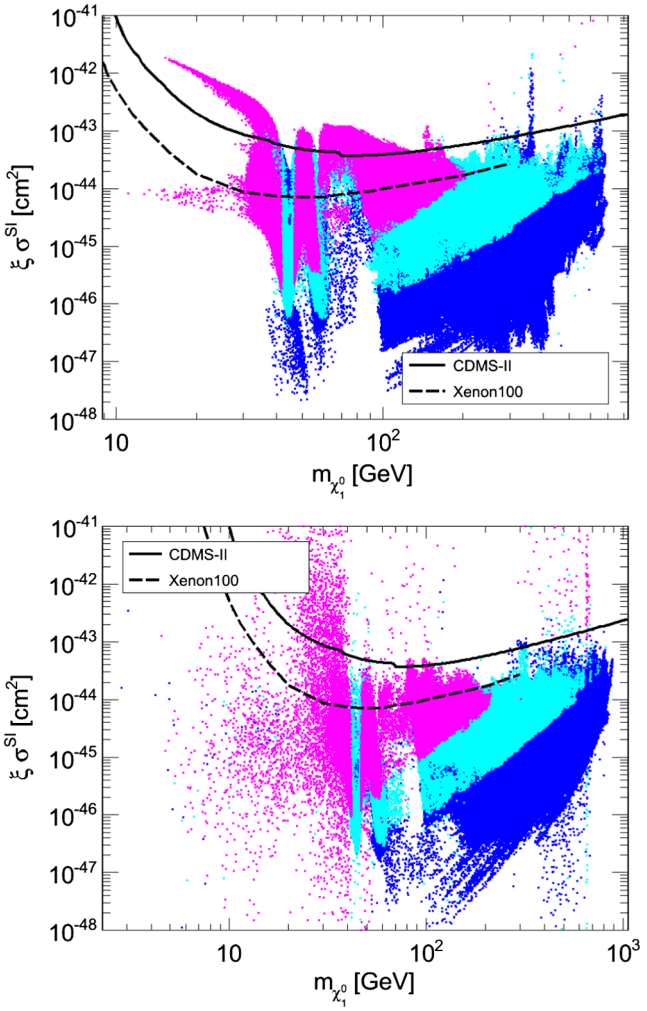

FIG. 4 (color online). Spin-independent cross section versus the neutralino mass. Top: MSSM. Bottom: NMSSM. In pink the points in the discovery region of directional detectors and in cyan in the exclusion region. The CDMS-II [23] and XENON100 [20] limits are also displayed.

Above 30 GeV, neutralinos can achieve the correct relic density by resonant Z exchange. That region (for $m_{\chi_1^0} \sim 45$ GeV) is well represented in both models. In both cases many points show small SI rates. Since the Z resonance enhances the annihilation rate, the $Z\chi_1^0\chi_1^0$ coupling should be suppressed, in order to have enough neutralinos left after the thermal freeze-out. Hence the Higgs couplings, which depend on the higgsino component of the LSP as the Z coupling, are also suppressed, which in turn diminishes the SI cross section. Above the Z resonance, and around

60 GeV, the SM-like Higgs exchange on resonance dominates the relic density. For the same reason, when the masses are very fine-tuned, $m_{\chi_1^0} \approx m_h/2$, the required annihilation rate forces the Higgs-neutralino coupling (responsible for the interaction) to be fairly small, therefore allowing very weak SI interactions. Note that the 45–85 GeV neutralino mass range with large cross sections is more populated in the MSSM than the NMSSM. This could be understood in terms of the couplings of the SM-like Higgs to the LSP which can be suppressed because of the singlet component in the NMSSM.

Approaching 100 GeV, neutralinos could have larger higgsino components, since we can have $\mu \gtrsim 100$ GeV $\sim m_{\chi_1^0}$. Furthermore there are many possibilities for neutralinos to achieve the relic density: by Z or Higgs exchanges (large higgsino components) or via sfermion and gaugino exchanges. Also, the heavier the neutralino, the narrower the neutralino-squark mass difference could be. This enhances the squark contribution and allows for some unusually large cross sections. The predictions for the SI cross section span 5 orders of magnitute. In general, the heavier the neutralino, the smaller the cross section and the XENON100 limits eventually do not constrain many configurations with $m_{\chi_1^0} < 200$ GeV.

2. Gamma rays

Neutralinos in Galactic objects, such as the Milky Way and its dSphS, have a probability of encountering and annihilating into SM fermions. After the subsequent decays and hadronization, these events produce γ rays. More marginally, γ rays can be produced from internal lines in the annihilation process or directly by pairs, the latter which occur through a loop-induced process that is not included in our flux computation. Among the indirect signatures, γ rays can be easily computed, as compared to charged cosmic rays, they do not suffer from energy losses and their propagation is not subject to uncertainties on the interstellar medium. Also, the Fermi-LAT, HESS and MAGIC experiments are successfully exploring the fluxes at Earth, thus providing means to constrain DM models.

The expected flux of γ photons of energy E for a given angular spread ψ, $\phi_\gamma(E, \psi)$ depends upon the square of the neutralino density, on the annihilation cross section $\langle \sigma v \rangle$ times the squared local abundance of neutralinos $\rho^2_{\chi_1^0}$ and on the particle spectrum produced $\frac{dN(E)}{dE}$. The computation of the flux implies the integral over the line of sight (l.o.s.) l within the extension of the desired area, which is usually matched to that of an observatory. Hence

$$\phi_\gamma(E, \psi) = \int_{\text{l.o.s.}} dl(\psi) \rho^2_{\chi_1^0}(l(\psi)) \times \frac{1}{2} \frac{\langle \sigma v \rangle}{4\pi m^2_{\chi_1^0}} \frac{dN(E)}{dE}$$
$$= J(\psi) \times \phi^{PP}(E).$$

We have explicitly split the so-called astrophysics term $J(\psi)$—namely the l.o.s. integral containing all the terms which carry spatial dependence—and particle physics term $\phi^{PP}(E)$—which is the energy-dependent term. The former can only be determined with the knowledge of the DM distribution in the observed object. We focus here on dSphs observed by Fermi-LAT [102], for which they provide an estimation of $J(\psi)$ (see their Table IV). We compute $\int \phi^{PP}(E)$ over the $[100\ \text{MeV}, \text{m}_{\chi_1^0}]$ interval. Here, we have scaled down the flux by a ξ^2 factor in order to take into account only the neutralino contribution to the DM density distribution.

The annihilation cross section at galactic velocities is related to the interaction rate at freeze-out. However, the velocity in galaxies is much lower than at freeze-out, hence large variations can take place when the annihilation occurs via resonances in the early universe [107]. In general annihilations that proceed through a Higgs and/or Z resonance in the early Universe are diminished at $v \sim 10^{-3}$ c, furthermore sfermion exchange into light fermions get suppressed. However it is also possible to have an enhancement of the neutralino annihilation cross section in galaxies when it is dominated by the exchange of a Higgs with a narrow width; see [101] for a discussion on this subject in the particular case of the light neutralinos in the NMSSM.

Figure 5 shows the γ-ray integrated flux expected from the Draco dSph as a function of the neutralino mass, along with the Fermi-LAT limits [102]. Color tagging in relation to detectability in directional detection will be discussed in Sec. V C. Fewer points are challenged by Fermi-LAT than by XENON100. Only the lighter configurations can be constrained by their γ-ray yield, while heavier neutralinos seem to be out of the reach of the Fermi-LAT detector. As for SI interactions, results for the MSSM and the NMSSM differ mainly for the lighter neutralino configurations. Here, the scalar Higgs exchanges suffer from a low-velocity suppression, while the pseudoscalar exchanges can be resonantly enhanced, this is possible only in the NMSSM. Thus, again, the NMSSM predicts a broader range of possible γ-ray yields when neutralinos are light. An order-of-magnitude enhancement of the Fermi-LAT sensitivity would probe all the configurations in the MSSM up to 30 GeV neutralino masses, and many scenarios up to 200 GeV in both models.

B. Predictions for spin-dependent interactions

The predictions for the $\xi\sigma_p^{\text{SD}}$ observable, which is the target of the future directional detectors, can be seen in Fig. 6. We also show the projected curves for the discovery limit (in pink), defined as a significance greater than the 3σ level at 90% C.L. in 30 kg · year CF_4 directional detector, and the exclusion limit (in cyan), in the background-free case for the same detector with the same exposure; see Sec. II. These curves define three regions: the discovery region above the discovery curve, the exclusion region

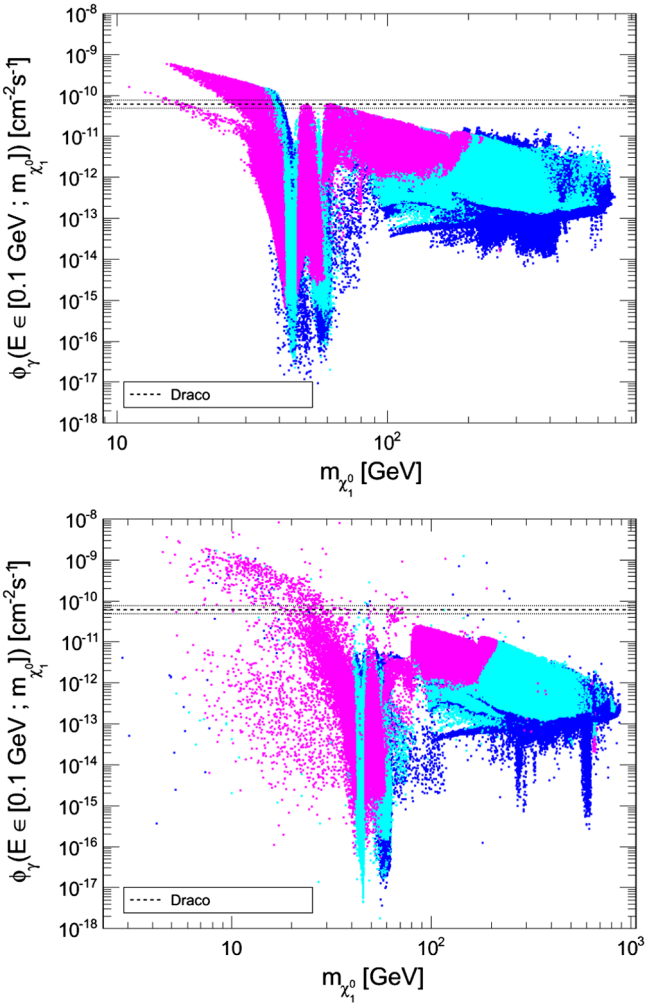

FIG. 5 (color online). Flux of γ rays expected from neutralino annihilations from the Draco dwarf spheroidal galaxy versus the neutralino mass. Top: MSSM. Bottom: NMSSM. In pink the points in the discovery region of directional detectors and in cyan in the exclusion region. The Fermi-LAT limits [102] are also displayed.

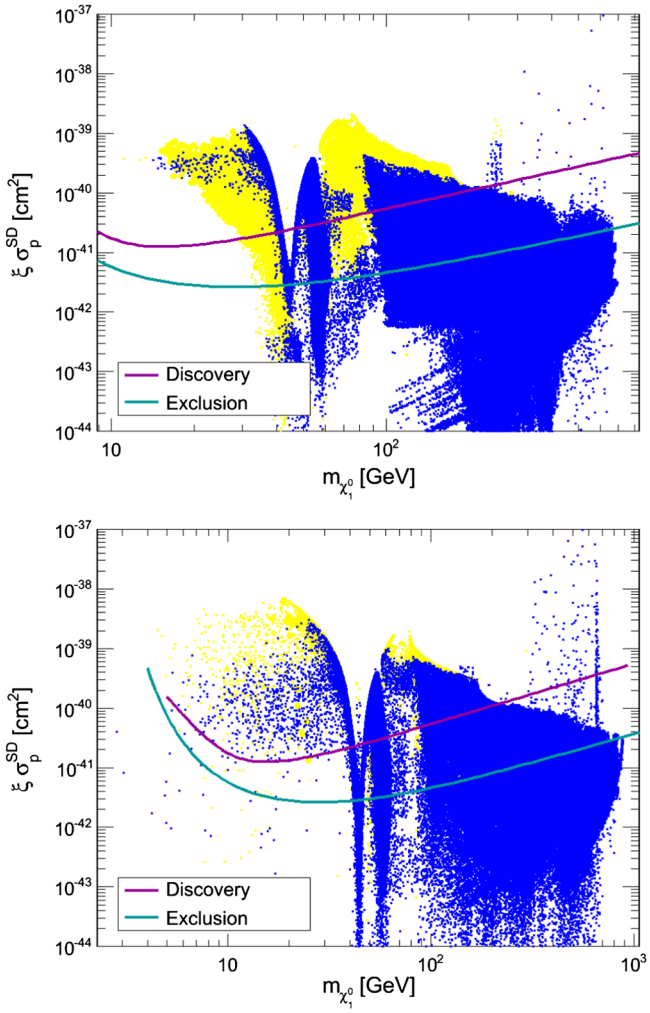

FIG. 6 (color online). Proton-neutralino spin-dependent elastic scattering cross section versus the neutralino mass with the exclusion and discovery projections for a nominal directional detector. Top: MSSM. Bottom: NMSSM. In blue safe points and in yellow points excluded by either XENON100 or Fermi-LAT.

between the two curves, and the out-of-reach region below the exclusion limit. We have tagged points failing to overcome the XENON100 and/or the Fermi-LAT constraints in yellow. MSSM and NMSSM configurations range over several orders of magnitude, the maximum reaches 10^{-39} cm^2 and a large fraction of the points lie above the potential exclusion limit of future directional detectors. One can readily see that some configurations that are not yet constrained by SI detectors nor by indirect signals (blue points) lie in the exclusion or even the discovery region.

In particular most neutralinos with a mass $m_{\chi_1^0} \leq 40$ GeV lead to large cross sections. This is understandable since in this case the same diagram (Z exchange) is responsible for both annihilation and scattering on nucleon. Enhancing the annihilation cross section in order to get an acceptable relic density implies enhancing the SD cross sections. However, when the neutralino mass approaches $m_Z/2$, the Z-neutralino coupling is reduced so the relic density is not too small, hence yielding very small SD interaction rates.

For larger neutralino masses, the possible cross section values range similarly to the SI case. However, here there is a clear upper limit for the SD, Z-exchange preferred configurations. For $m_{\chi_1^0} \geq 100$ GeV the SD cross section scales as $1/m^2_{\chi_1^0}$. Also, the largest coupling between the Z and the neutralino is $\mathrm{Max}(N_{13}^2 - N_{14}^2) = 0.5$, which can be met for higgsino-dominated neutralinos. Those configurations having the maximum coupling describe the upper limit of the cloud above 70 GeV, drawing the $1/m^2_{\chi_1^0}$ curve. Points falling above that limit imply dominant squark exchanges, and points below have either smaller couplings or destructive interference between the Z and squark

exchange diagrams. It is worth emphasizing that in the MSSM, and to a lesser extent in the NMSSM, a large fraction of the supersymmetric configurations below $m_{\chi_1^0} \leq 200$ GeV lies in the discovery region, meaning that such models could be discovered, with a significance greater than 3σ (90% CL), with a 30 kg · year CF_4 directional detector. Exclusions may be reached up to ~800 GeV.

As outlined in Sec. III, a model-independent constraint on DM requires us to present the results in the $(\sigma_p^{\mathrm{SD}}, \sigma_n^{\mathrm{SD}}, m_\chi)$ parameter space.[3] In order to have a complete view of the theoretical predictions, we present in Figs. 7 the σ^{SD} on proton versus neutron, for all neutralino masses. The discovery (resp. exclusion) limit depends on the mass, ranging from $\sim 2 \times 10^{-41}$ cm^2 ($\sim 7 \times 10^{-42}$ cm^2) for a ~10 GeV WIMP to $\sim 2 \times 10^{-40}$ cm^2 ($\sim 2 \times 10^{-41}$ cm^2) for a ~500 GeV WIMP. Color tagging refers to the detectability in directional detection: pink discovery region, cyan exclusion region and blue out-of-reach. As expected, in models dominated by Z exchange, we found $\sigma_p/\sigma_n = 1.3$ (see Sec. III A). Most of the points in the discovery region (pink points) satisfy this condition. Exceptions are points where $N_{13}^2 - N_{14}^2$ is small and the squarks are light (more specifically below 300 GeV). The latter could easily be excluded by the LHC, unless they are degenerated with neutralinos; see Sec. VI for a more complete discussion on that respect.

When the squark exchange comes into play, interference between the squark and Z contributions can reduce either the neutron or proton cross sections, and the correlation is lost. Indeed, when the Z exchange is dominant but the squark exchange becomes non negligible, the proton cross section is lessened rather than the neutron cross section (points deviating from the correlation line towards the bottom). When the Z and squark exchanges are similar, then the destructive interference can completely erase one or the other of cross section, but not both, depending on the nature of the lightest squark. These cases correspond to the broad vertical (proton cross section suppression) and horizontal (neutron cross section suppression) distributions towards smaller cross sections in the top panel of Fig. 7. Finally, when the squark exchange dominates, the proton cross section being favored, the correlation reaches $\sigma_p/\sigma_n = 11.4$ (see Sec. III A). In the NMSSM the correlation $\sigma_p/\sigma_n = 1.3$ extends to lower values of the cross section. In such a case the neutralino is dominantly higgsino with a significant singlino component, furthermore $N_{13} \approx N_{14}$ so that the Z contribution is suppressed, hence the low cross section. The annihilation of neutralinos in the early Universe is driven by the singlino component and the Higgs sector. Such scenarios are more difficult to obtain in the MSSM, furthermore the lower bound on the relic density constrains the case of a dominantly higgsino LSP.

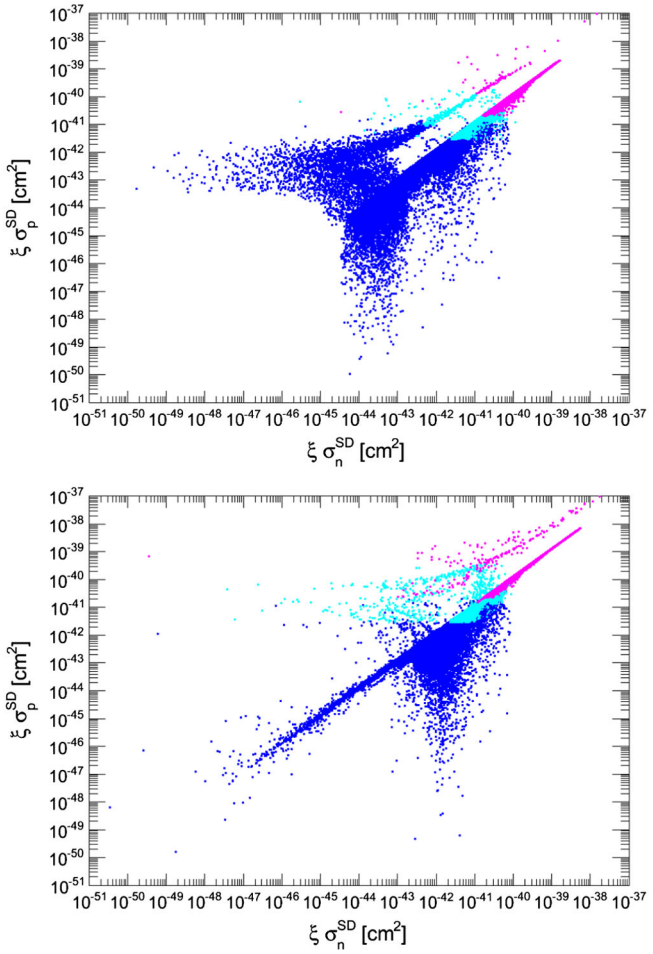

FIG. 7 (color online). Spin-dependent elastic scattering cross sections correlations: proton-neutralino versus neutron-neutralino interactions. Contrarily to Fig. 3, the result is presented for all neutralino masses. Top: MSSM. Bottom: NMSSM. In pink the points in the discovery region of directional detectors and in cyan in the exclusion region.

Figure 8 presents the frequency distribution of a_p/a_n for the points of Fig. 7 with the same color code. As outlined in Sec. III B, the relative sign of a_p and a_n is a key issue for SD direct searches. Indeed the interference can be either constructive or destructive, depending of the sign of the spin contents of the target nucleus [see Eq. (6)]. For both the MSSM and the NMSSM we observe that most models give $a_p/a_n \simeq -1.13$, corresponding to a dominant Z exchange. A small number of models give $a_p/a_n \simeq -3.5$, corresponding to a squark ($\tilde{q}_R$) contribution in the pure bino limit. However, amplitudes can also be of the same sign. As we shall see in Sec. VI, this is not the case when applying recent ATLAS limits on squarks and gluinos.

[3]Note however that it requires us to set the SI coupling to zero, which is not model-independent *stricto sensu*.

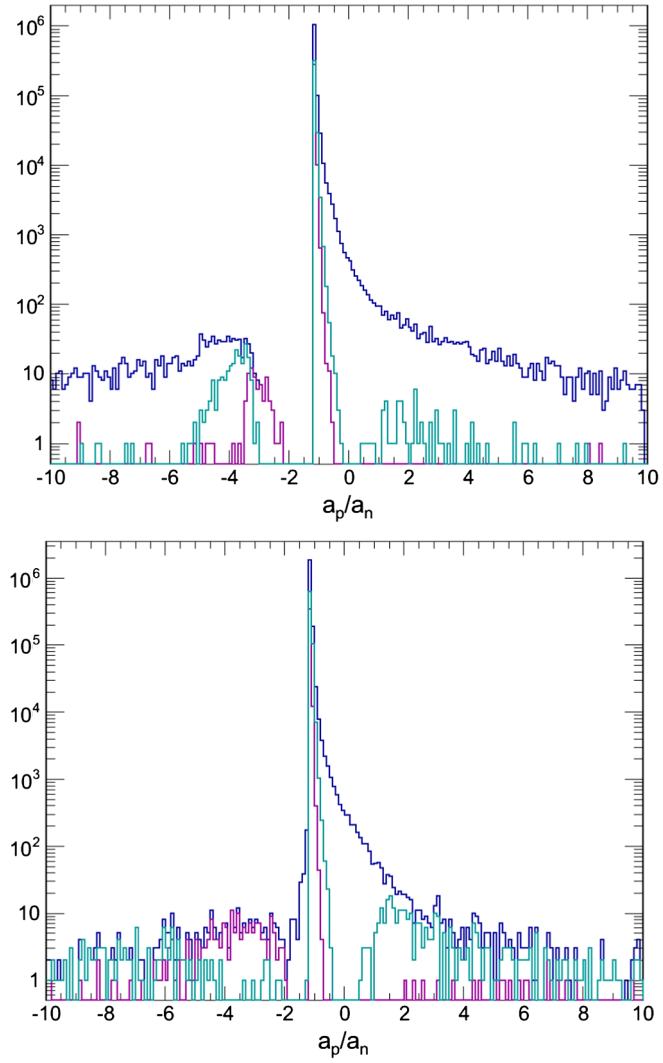

FIG. 8 (color online). Frequency distribution of ap/an. Top: MSSM. Bottom: NMSSM. In pink the points in the discovery region of directional detectors and in cyan in the exclusion region.

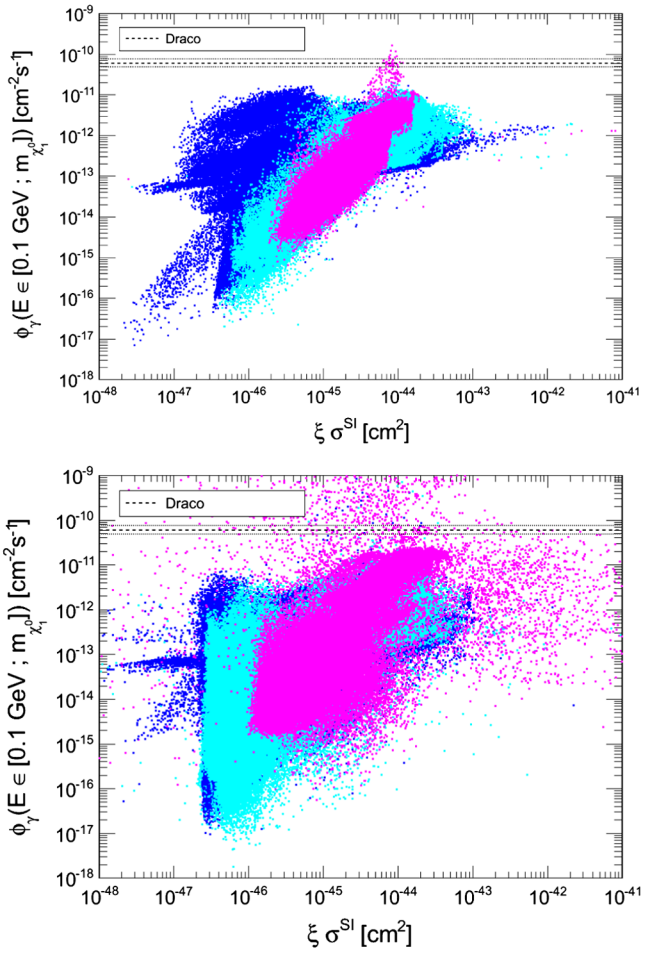

FIG. 9 (color online). Flux of γ rays expected from neutralino annihilations from the Draco dwarf spheroidal galaxy versus spin-independent cross section. Top: MSSM. Bottom: NMSSM. In pink the points in the discovery region of directional detectors and in cyan in the exclusion region. The Fermi-LAT limits [102] are also displayed. Points excluded by XENON100 are not shown.

C. The complementarity between directional detectors and other techniques

We have already shown in Sec. V B that directional detectors will scan an important fraction of the supersymmetric parameter space. We have also shown the power of XENON100 (in direct SI detection) and Fermi-LAT (in indirect detection experiments) to put constraints on neutralino DM configurations in Sec. V A. For the NMSSM case, it has been discussed in [101] that SI direct detection and indirect detection of γ rays constrain different light neutralino scenarios. In particular the light scalar Higgs case is reachable by the former, while light pseudoscalar configurations are probed by the latter.

Let us discuss the impact of SD direct detection searches and their position in this sense. Figures 4 and 5 show the yields in SI cross sections and in γ rays from the Draco dSph, respectively. In these planes we have tagged in pink the scenarios that fall in the discovery region of future directional detectors, in cyan scenarios between the exclusion and the discovery curves, and in blue those points which are not expected to produce enough signal. In both cases one can see that there are many pink points below the exclusion limits of XENON100 (in Figs. 4) and below those of Fermi-LAT (in Figs. 5). Most of these pink points correspond to $m_{\chi_1^0} \leq 200$ GeV. We can observe that the development of a SD directional detector will help closing the parameter space that seems to escape other techniques. Unfortunately, we also observe many blue points in both figures, which lie orders of magnitude below the reach of all DM search strategies.

We summarize the complementarity of detection techniques in Figs. 9, in which we show the correlation between SI and indirect detection techniques, using the color

tagging for the directional detectors potential reach. Those points failing to satisfy the XENON100 limit (which cannot be represented in this plane) are not drawn. Notice that the pink cloud, set to be up front, covers a large region of this correlation plane, spanning over more than 2 (7) orders of magnitude in the $\xi\sigma^{\mathrm{SI}}$ axis, and over more than 5 (7) orders of magnitude in the ϕ_γ axis for the MSSM (NMSSM). This, of course, includes many configurations that are not only far away from the current reach of SI and indirect detectors, but that would also escape their forthcoming upgrades. Supersymmetric models with neutralino DM candidates predict possible configurations in the range of detection for all the experimental techniques exposed here. However, it is obvious that none is able by itself to probe every configuration we found. Indeed, the reach of any of these techniques alone is frustratingly insufficient. In this sense, the development of SD detection techniques is useful for a thorough scan of neutralino DM supersymmetric configurations. In particular, the superposition of the blue, cyan and pink clouds in Figs. 9 leads us to conclude that the capability of SD directional detection, either to discover or to exclude a DM model, is not correlated with the sensitivity of the SI and indirect searches. It does, in particular, highlight the complementarity of the various DM search strategies.

D. Constraining MSSM and NMSSM parameter spaces with directional detectors

Although the MSSM and NMSSM parameter spaces are multidimensional and can produce many different phenomenologies, the reach of directional detectors is determined solely by the DM particle mass and the SD cross section. In particular, for masses below 200 GeV, a large fraction of the supersymmetric configurations fall in the discovery region. For neutralinos to satisfy $m_{\chi_1^0} \leq$ 200 GeV, the mass term of at least one of its components has to satisfy the same condition. This can be either the bino component determined by M_1, the higgsino component given by μ, the wino component given by M_2 or the singlino component in the NMSSM (which depends on a combination of λ, κ and μ). Note however that when the neutralino LSP is wino-dominated, which implies $M_2 \leq M_1$, μ, the relic density tends to be very small, those configurations are therefore excluded by the condition $\Omega_{\chi_1^0}h^2 \geq 10\%\Omega_{\mathrm{WMAP}}h^2$. The neutralino LSP main component is therefore determined by the lighter of M_1, μ. The strength of the SD interactions, strongly depend on the μ value, determining the neutralino mixing elements N_{13} and N_{14}, thus the $Z\chi_1^0\chi_1^0$ coupling. Since the lighter the μ the larger $|N_{13}|$ and $|N_{14}|$, the lighter the neutralino (although depending on M_1, and the singlino component in the NMSSM), we expect small μ values to be generally in the reach of directional detectors.

In Fig. 10 we present the correlation between μ and M_1, using the same color tag for points in or out the discovery and exclusion regions. The general trend just discussed is indeed met: a discovery is mostly linked with $\mu \lesssim$ 250–300 GeV. Roughly speaking, the $\mu = M_1$ line separates the bino- and higgsino-dominated neutralino compositions.

For a binolike neutralino to have large enough SD interactions (pink or cyan points), either the higgsino component is not negligible (i.e., points above the $\mu = M_1$ line but not far away from it), either the squarks have similar masses to those of neutralinos (which is the case of the few pink and cyan points above and far away from the $\mu = M_1$ line). The former case is very well represented by the vertical clouds at $M_1 \sim 50$ GeV, corresponding to annihilation via the Z resonance. In such a line, μ below 300 GeV allows discovery (pink points), and up to ~450 GeV the configurations could be challenged by directional detectors (cyan points). Larger values of μ would be out of reach (blue points).

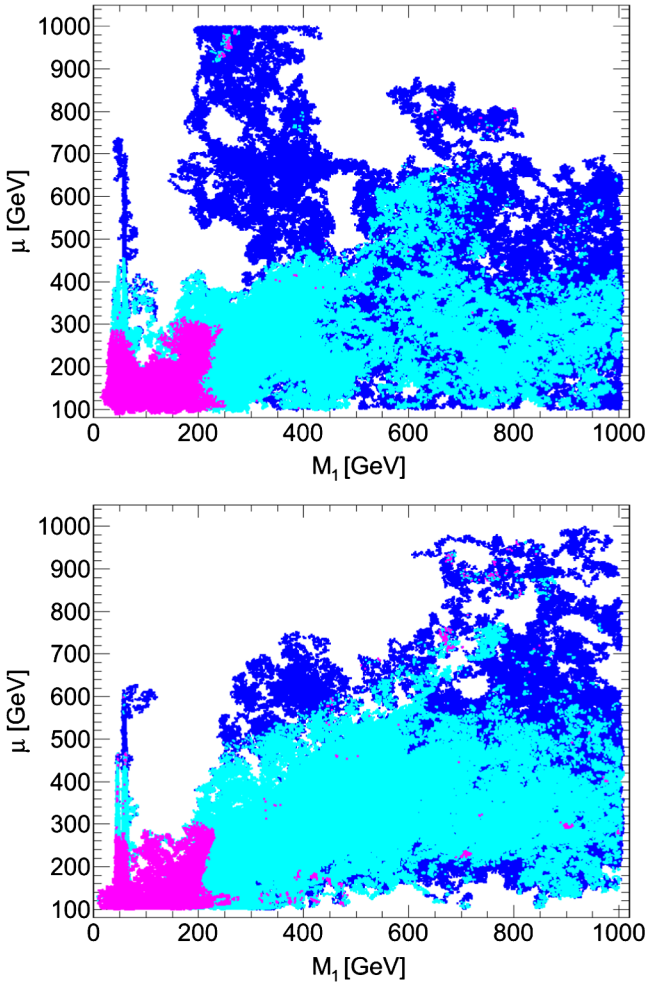

FIG. 10 (color online). Correlation plot between the μ mass term and the bino mass M_1. Top: MSSM. Bottom: NMSSM. In pink the points in the discovery region of directional detectors and in cyan in the exclusion region.

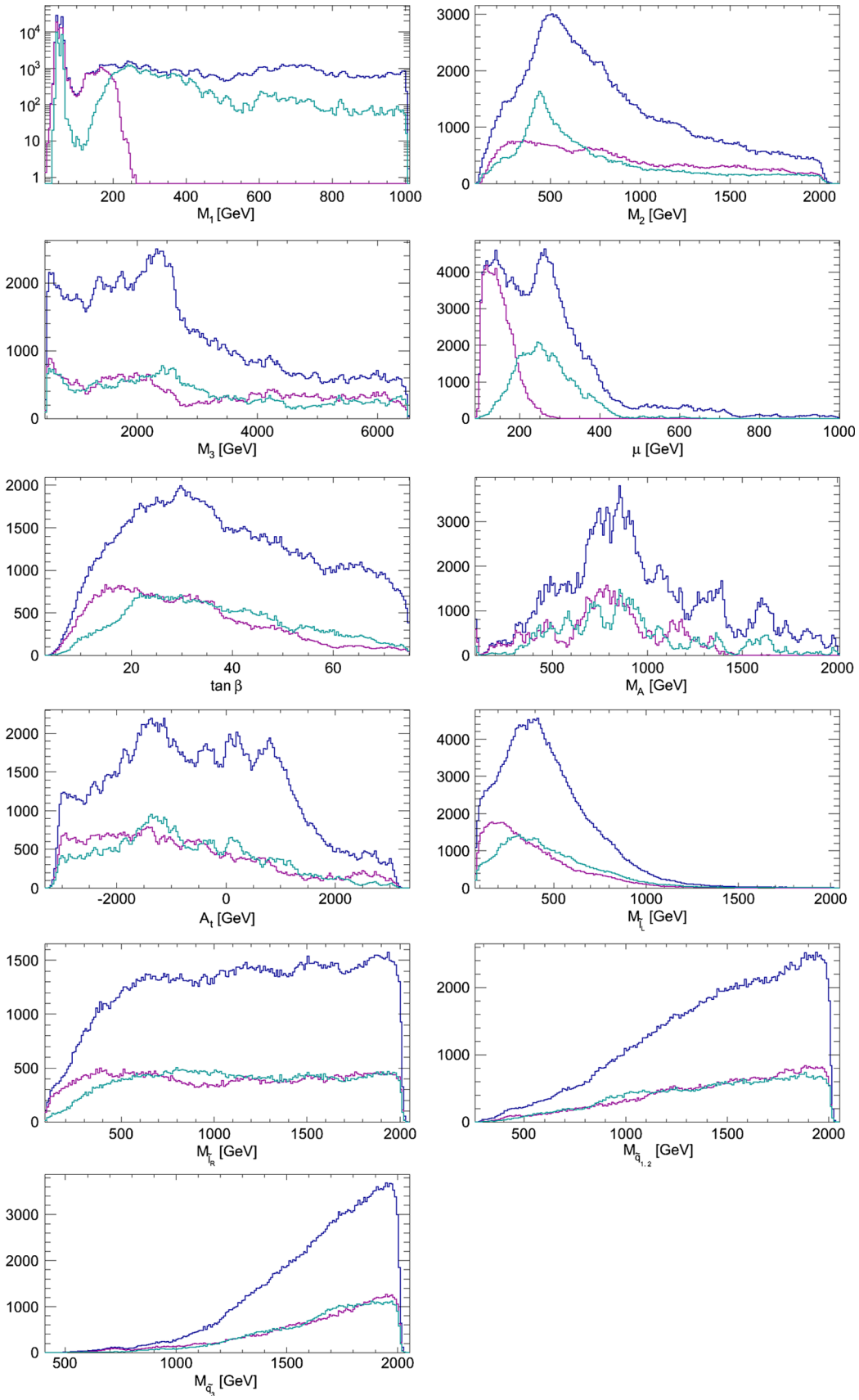

FIG. 11 (color online). Free parameter frequency distribution normalized to $\mathcal{Q}_{\max}$ in the MSSM run. In pink the points in the discovery region of directional detectors and in cyan in the exclusion region.

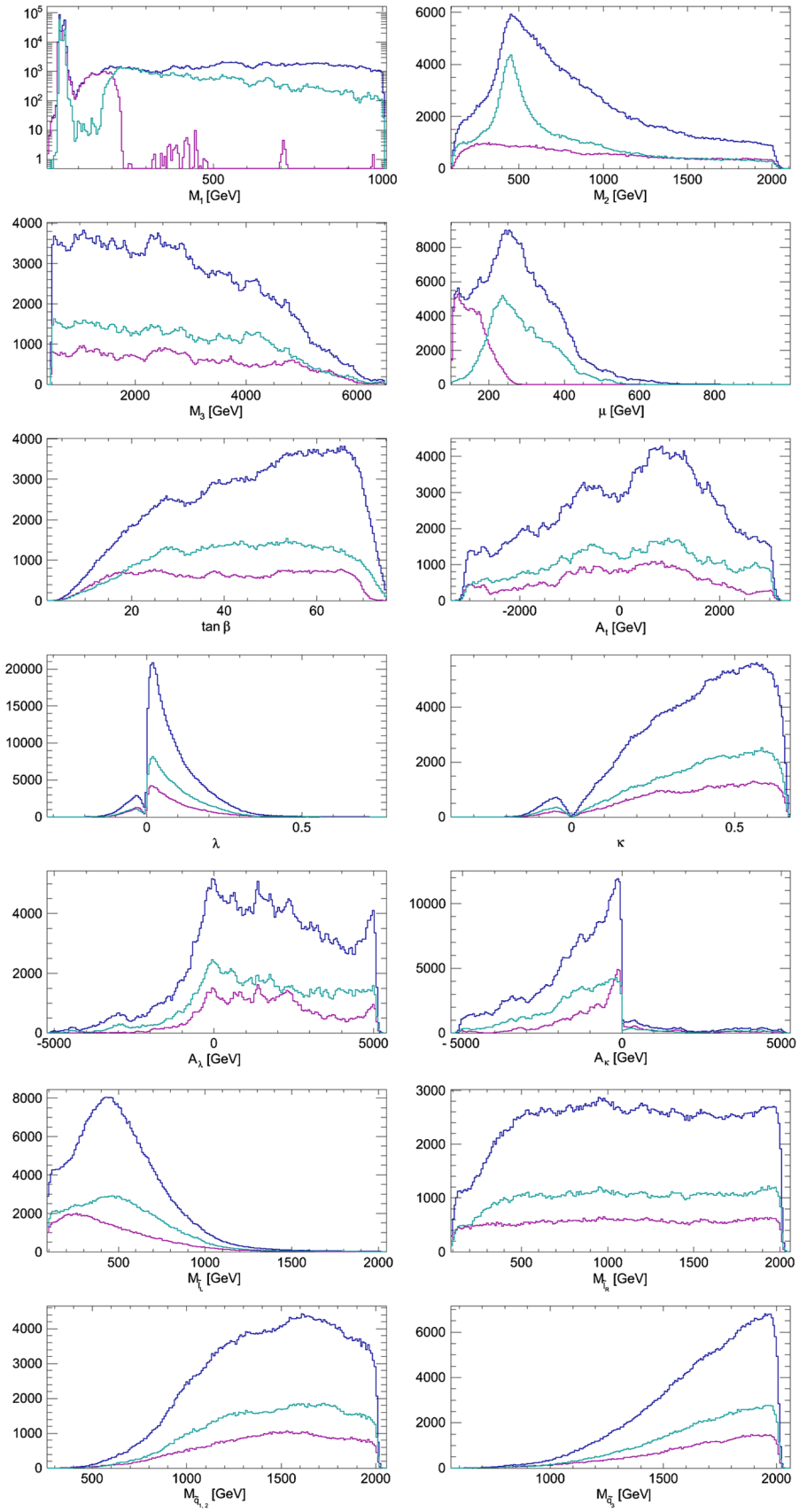

FIG. 12 (color online). Free parameter frequency distribution normalized to $\mathcal{Q}_{\max}$ in the NMSSM run. In pink the points in the discovery region of directional detectors and in cyan in the exclusion region.

The effect of the neutralino mass is imprinted in the fact that very few pink points can be found at large values of M_1 and μ. This is easily understood: the heavier the neutralino, the smaller the cross section and the smaller the projected sensitivity, the less configurations fall in the discovery region.

The correlation between small values of μ and the discovery potential is also observed in Figs. 11 and 12. In these figures we show the frequency distribution of all free parameters in the MSSM and NMSSM, respectively, for all points (blue), as well as for pink and cyan points only. In the fourth panel of both figures one can see that the pink distribution of μ is strongly peaked towards the lighter values, almost reaching the all point curve in the MSSM. Indeed, few configurations with $\mu \leq 150$ GeV would actually escape a discovery with a large directional detector (30 kg · year). In the NMSSM such configurations could also have a large singlino component in which case they would remain out of reach of directional detectors. Regarding M_1 (first panel), the pink and cyan distributions also reflect the neutralino mass range for detection and exclusion. In particular, apart from some configurations with M_1 around $M_Z/2$ (Z resonant neutralinos), most configurations with $M_1 \lesssim 450$ GeV would be challenged by future directional detectors. Conversely, for μ, $M_1 \geq 450$ GeV, most supersymmetric configuration would not be probed by directional detectors, even if exclusion remains possible.

As for the other parameters, the shapes of distributions are to a large extent related to the LSP mass. The exclusion region does not contain any points with a LSP lighter than 35 GeV and extends to much larger masses for the LSP than the discovery region. Thus the cyan distributions for the masses of supersymmetric particles will be shifted towards higher values than the pink distributions. In particular the distributions for the soft terms μ, M_2 that drive the masses of the neutralinos and charginos are peaked at higher values for the exclusion region than for the discovery region. For the same reason, the pink distribution for $M_{\tilde{l}_L}$ and $M_{\tilde{l}_R}$ are shifted towards smaller values than the cyan and blue distributions. Regarding $\tan\beta$, we also expect to see that smaller values are preferred for the points in the discovery region. Indeed, in the MSSM, the light neutralino LSP is often associated with a light M_A, collider constraints on the Higgs sector then selects small values of $\tan\beta$. This trend is also met in the NMSSM, however, since the light neutralino is not necessarily associated with a light pseudoscalar mass, there is a much larger fraction of configurations with small values of $\tan\beta$ that escape SD detectability. Finally we remark that the masses of squarks and gluinos can extend well above 1 TeV, this sector is mostly constrained by flavour observables. Therefore a large fraction of the configurations will escape detection at the LHC as will be discussed next.

VI. IMPACT OF LHC RESULTS ON THE PARAMETER SPACE

The ATLAS collaboration has published an analysis and established a limit on the squark mass versus gluino mass plane [74]. These limits were derived for massless neutralino LSP in the MSSM and assuming that the squarks decay exclusively into a quark and the LSP. This is not the case in the scans we have performed in the MSSM, in particular, additional decay modes of the squarks can weaken the ATLAS limits. However, comparing these limits to our data sets is a good way to check the possible influence of the forthcoming results of the LHC in terms of parameter space cutting and its implications for SD cross sections. The modification of the squark decay modes and the presence of light Higgs states mean that these limits do not apply to the NMSSM, thus we restrict this analysis to the MSSM.[4]

We have applied the limit on the $M_{\tilde{q}}$ vs $M_{\tilde{g}}$ plane, where $M_{\tilde{q}}$ stands for the lightest first- or second-generation squark mass. Points falling below the curve provided by ATLAS are not represented in Fig. 13 (top panel), where we show the correlation between neutralino SD interactions with protons and neutrons. The difference is quite striking with respect to the top panel in Fig. 7, where all points are drawn. What we observe is that, as the LHC probes the lightest squarks (in the hypothesis these are not observed), only the points in the main correlation line are left. Thus, the possibilities to achieve a large SD interaction would be restricted to a large higgsino fraction. Bottom panel of Fig. 13 presents the frequency distribution of a_p/a_n for the same points with the same color code. As outlined in Sec. III B, the relative sign of a_p and a_n is a key issue for SD direct searches. It is worth noticing that taking into account recent ATLAS limits on squarks and gluinos restricts the allowed models to the ones with negative values of a_p/a_n. More precisely, only the Z exchange is allowed, and the ratio of the two amplitudes is given by $a_p/a_n \simeq -1.14$ (see Sec. III A). It implies that a nucleus target with spin contents of opposite sign (e.g., ^{19}F, ^{3}He or ^{133}Cs) will present a constructive interference while nucleus target with spin contents of same sign (e.g., ^{129}Xe, ^{131}Xe or ^{73}Ge) will have a destructive interference thus reducing the cross section on nucleus and hence the event rate. A dedicated study is needed on this issue, but we emphasize that it may have consequences in the choice of target for upcoming SD experiments. Note that this statement is rather independent of the details of the SUSY model, as long as LHC exclusions on squarks apply.

[4]An analysis of the ATLAS constraints on the NMSSM parameter space is ongoing [108].

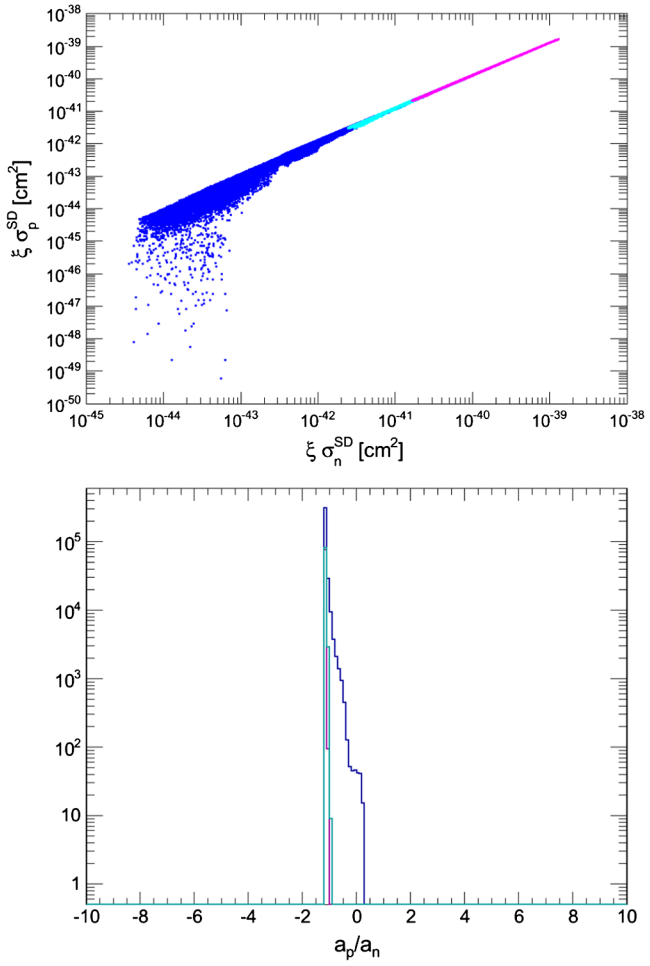

FIG. 13 (color online). Top Panel: Spin-dependent elastic scattering cross sections correlations: proton-neutralino versus neutron-neutralino interactions in the MSSM. In pink the points in the discovery region of directional detectors and in cyan in the exclusion region. Here, in contrast with Figs. 7, we have removed those points falling above the ATLAS limit on the $M_{\tilde{q}}$ vs $M_{\tilde{g}}$ plane. Bottom panel: frequency distribution of a_p/a_n for the same points with the same color code.

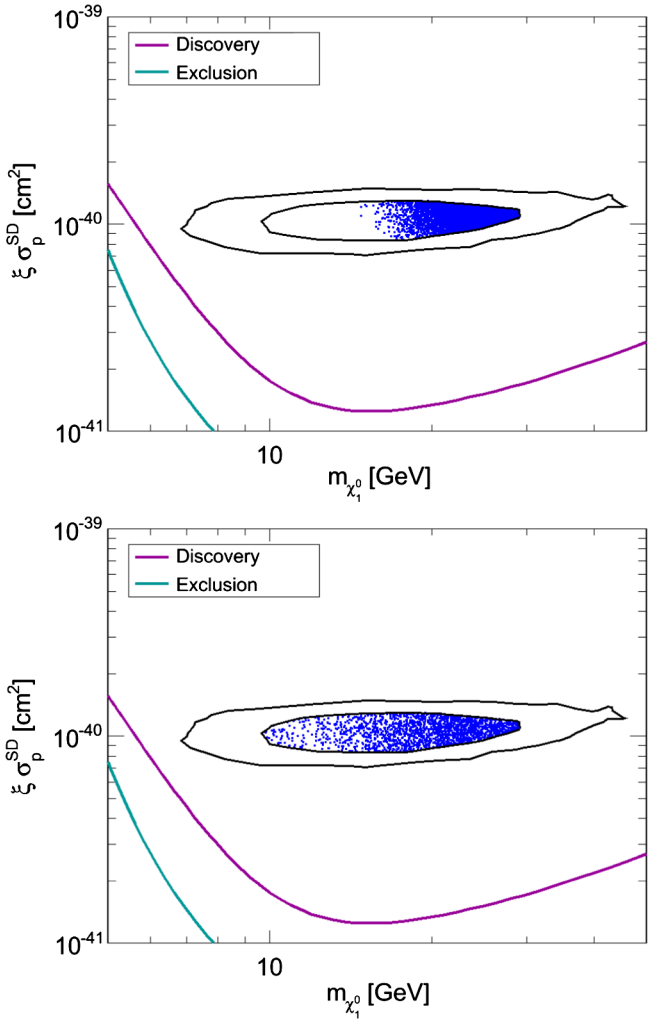

FIG. 14 (color online). Proton-neutralino spin-dependent elastic scattering cross section versus the neutralino mass in the discovery scenario runs. Top: MSSM. Bottom: NMSSM. We display the 1σ and 3σ contours, while we used the former as the constraint for the random walk. Also displayed are the exclusion and discovery projections for a nominal directional detector. We display only safe points regarding XENON100, Fermi-LAT and CMS (MSSM only) limits on SI elastic scattering interactions, γ rays from the Draco dSph, and Higgs interactions.

VII. A DISCOVERY SCENARIO

As outlined in Sec. II B 2, a dedicated analysis of data of a 30 kg · year CF_4 directional detector could also allow us to constrain the WIMP properties, both from particle physics (m_χ, σ_p^{SD}) and galactic halo (velocity dispersions) [9]. This would be one step beyond current DM search strategy capabilities. Of course, this requires a rather large SD cross section associated with a low neutralino mass. The outcome would be a constraint on the mass and the cross section, i.e., within a contour defined by a confidence level.

In light of such a tool, we perform the following exercise [9]: we assume the existence of a DM particle of 20 GeV mass with 10^{-4} pb interaction rate with protons, leading to ≈ 80 WIMP events in a 30 kg · year CF_4 directional detector, to generate simulated data. Then, we infer the contour from the data analysis procedure after detection by a canonical directional detector. We exploit this result by including a new prior in the MCMC described in Sec. IV B: we impose the neutralino mass and the SD cross section to lie in the 1σ contour obtained by the discovery. Hence, we are able to scan the possible scenarios fitting the observation.

In Fig. 14 we show the distribution of points within the contour in the SD vs neutralino mass plane. Notice that the transition in the contour prior was sharp, so no point is kept outside those boundaries. In the NMSSM (bottom panel), we have much less statistics than in the MSSM (top panel), however, populating this discovery

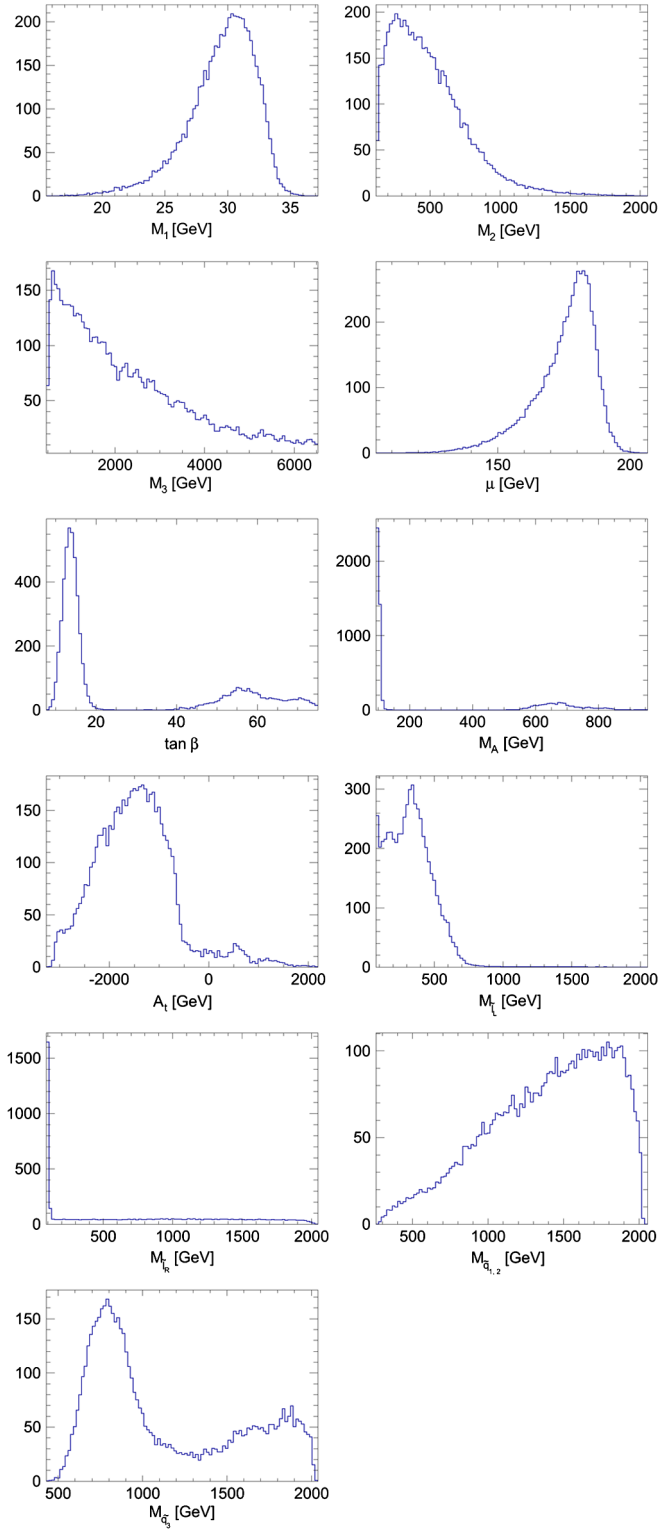

FIG. 15 (color online). Free parameter frequency distribution normalized to $\mathcal{Q}_{\max}$ in the MSSM discovery scenario run.

region more is only a matter of time. Nevertheless, the contour is much more homogeneously filled in the NMSSM case, showing that there are more possibilities to find good configurations, in contrast with the MSSM

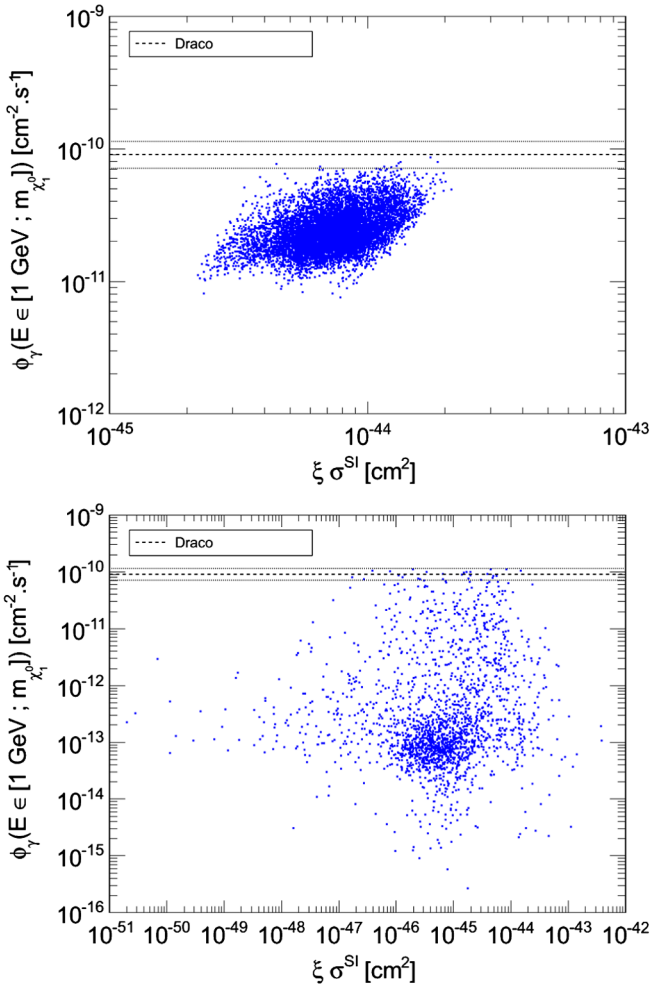

FIG. 16 (color online). Flux of γ rays expected from neutralino annihilations from the Draco dwarf spheroidal galaxy versus spin-independent cross section. Top: MSSM. Bottom: NMSSM. The Fermi-LAT limits [102] are also displayed. Only the points overcoming all constraints (from XENON100, Fermi-LAT and CMS) in the discovery scenario are displayed.

where the heavy end of the contour is much more preferred than the actual value of the WIMP in the simulation input. Hence, the NMSSM neutralino DM appears a much more plausible explanation if such a detection was made. In these figures we have kept only the points that satisfied all constraints including the CMS limits on $\tan\beta$ vs M_A plane (MSSM only) as well as Fermi-LAT and XENON100 limits.

An observation would allow us cto refine the expectations on the soft SUSY parameters, as can be seen by comparing the parameter distribution in Fig. 11 with the one corresponding to points in the contour in Fig. 15 in the case of the MSSM. Most distributions are determined by the condition on the neutralino LSP mass. This is clearly the case for M_1 which drives the mass of the light bino, but it also applies to other parameters [55]. Indeed for a light LSP to be consistent with the relic

density constraint requires either a light slepton, hence the very peaked distribution in for $M_{\tilde{l}_R}$ or a light Higgs boson, hence the peak in the M_A distribution. Higgs and flavor physics constraints then imply that intermediate values of $\tan\beta$ are disfavored. Furthermore the squark contribution that is needed to cancel the Higgs contribution in $B(b \to s\gamma)$ explains the peak at low values of the third-generation squark masses $M_{\tilde{q}_3}$. The main impact of imposing a specific range for σ^{SD} is reflected in the distribution for μ, confined to be in a narrow range. As mentioned previously, the strength of the neutralino coupling to the Z is the most relevant parameter in computing σ^{SD}.

Figs. 16 represent the safe points in the γ rays from Draco vs SI interaction plane. There is a concentration of points at 10^{-46}–10^{-45} cm^2 cross sections and 10^{-13} cm^3 s^{-1} fluxes. This constitutes the prediction for other detection techniques in case an observation is made. Because of the interplay of parameters, the spread of these predictions is rather large in the NMSSM: 9 orders of magnitude in the SI axis and 6 orders of magnitude in ϕ_γ. An order of magnitude spread is predicted in the MSSM. This is an extremely different behavior of the two models. Such a discovery would predict a MSSM neutralino to be found shortly by direct detection and indirect detection experiments, thus providing a cross check of the discovery claim. On the contrary, a NMSSM neutralino could easily escape any other detection.

TABLE V. Best $\mathcal{Q}$-weighted point in the MSSM (second column); best $\mathcal{Q}$-weighted (third column) and a low $\tan\beta$ point (fourth column) in the NMSSM (GeV units).

Parameter/Characteristics	MSSM	NMSSM 1	NMSSM 2
$\mathcal{Q}$	0.49	0.60	0.58
$M_{\chi_1^0}$	27.7	21.7	13.8
$\Omega_\chi h^2$	0.094	0.048	0.071
$\sigma_p^{\mathrm{SD}}[10^{-40}\ \mathrm{cm}^2]$	1.30	2.44	1.61
$\xi\sigma_p^{\mathrm{SD}}[10^{-40}\ \mathrm{cm}^2]$	1.11	1.07	1.04
M_1	30.6	25.8	6.0
M_2	500.4	1951.0	263.0
M_3	1115.6	1753.4	3487.5
μ	178.4	138.1	146.8
$\tan\beta$	46.6	51.9	7.2
M_A	814.4	-	-
λ	-	0.140	0.480
κ	-	0.032	0.013
A_λ	-	3308.1	1210.4
A_κ	-	−25.9	−82.5
A_t	−313.4	2491.1	−380.9
$M_{\tilde{l}_R}$	351.0	217.4	132.4
$M_{\tilde{l}_L}$	91.55	1990.3	947.2
$M_{\tilde{q}_{1,2}}$	1659.7	1707.2	1384.7
$M_{\tilde{q}_3}$	1842.6	1833.2	1938.7

In any case, keep in mind that such a discovery would still mean that $\mu \lesssim 200$ GeV, and $10\ \mathrm{GeV} \lesssim m_{\chi_1^0} \lesssim 30$ GeV. With these two characteristics we can predict the presence of a chargino with $m_{\chi_1^+} \lesssim 200$ GeV. A light slepton would be favored in the MSSM case, but its absence leaves only the NMSSM as a possibility. With the help of collider physics, it could be possible to rule out the possibility of a MSSM neutralino DM, or even of any supersymmetric neutralino if no charged particle is observed in the vicinity of the weak scale.

In Table V we present the best points found in both runs. Only points safe regarding XENON100, Fermi-LAT, and for the MSSM, CMS are taken into account. This restricts the MSSM points to the large $\tan\beta$, light slepton exchange case, and all other safe points are rather similar to the one we show. On the contrary, in the NMSSM there are quite different configurations in good agreement with all observations and the discovery hypothesis. Hence we show the best point along with an example of a good point with different characteristics.

VIII. CONCLUSION

We have shown that supersymmetric models with neutralino DM predict signals in the range of detection for SI and SD direct detectors as well as for indirect detectors. However only a fraction of the parameter space of either the MSSM or the NMSSM can be probed by each type of experiments alone. The development of SD directional detection techniques thus offer the possibility to probe more thoroughly the parameter space of supersymmetric models. This is the case even if the sensitivity of indirect detectors as well as SI detectors is increased by 1 order (or more) of magnitude, thus emphasizing the complementarity between different techniques.

With the planned MIMAC detector, neutralinos up to 200 GeV could be discovered and up to 600 GeV could be excluded. The light neutralinos that are best probed by directional detectors are often accompanied by not-so-heavy charginos/neutralinos and even sleptons or by a light pseudoscalar. The search for these weakly interacting particles at the LHC will therefore impact in the future the potential of directional detection to probe supersymmetric models. We expect the LHC to considerably expand the constraints on supersymmetric scenarios in the next year, even if no signal of physics beyond the standard model is found. We have shown that if squarks of the first two generations are excluded up to a mass of nearly 750 GeV, notwithstanding that they could escape detection due to small mass splittings with some other supersymmetric particles, the squarks play little role in direct detection and the SD cross section on protons is completely correlated with that on neutrons. The LHC is also probing supersymmetric models with Higgs searches, in particular, the negative search results on the heavy Higgs doublet of the MSSM constrain the supersymmetric models with a

light neutralino. Furthermore a confirmation of a Higgs signal at 125 GeV as announced by ATLAS would narrow down the number of allowed supersymmetric configurations. Note however that the light Higgs is not directly linked with SD direct detection.

ACKNOWLEDGMENTS

G. B. thanks the LPSC where part of this work was done, for its hospitality. D. A. V. thanks Céline Bœhm for very useful discussions and advice.

[1] M. Persic, P. Salucci, and F. Stel, Mon. Not. R. Astron. Soc. **281**, 27 (1996).
[2] A. Klypin, H. Zhao, and R. S. Somerville, Astrophys. J. **573**, 597 (2002).
[3] G. Bertone, *Particle Dark Matter: Observations, Models and Searches* (Cambridge University Press, Cambridge, England, 2010), p. 738.
[4] D. N. Spergel, Phys. Rev. D **37**, 1353 (1988).
[5] J. Billard, F. Mayet, J. F. Macias-Perez, and D. Santos, Phys. Lett. B **691**, 156 (2010).
[6] J. Billard, F. Mayet, and D. Santos, Phys. Rev. D **85**, 035006 (2012).
[7] A. M. Green and B. Morgan, Phys. Rev. D **81**, 061301 (2010).
[8] J. Billard, F. Mayet, and D. Santos, Phys. Rev. D **82**, 055011 (2010).
[9] J. Billard, F. Mayet, and D. Santos, Phys. Rev. D **83**, 075002 (2011).
[10] S. Ahlen *et al.*, Int. J. Mod. Phys. A **25**, 1 (2010).
[11] E. Behnke *et al.*, Phys. Rev. Lett. **106**, 021303 (2011).
[12] J. Angle *et al.*, Phys. Rev. Lett. **101**, 091301 (2008).
[13] V. N. Lebedenko *et al.*, Phys. Rev. Lett. **103**, 151302 (2009).
[14] M. Felizardo *et al.*, arXiv:1106.3014.
[15] A. Benoit *et al.*, Phys. Lett. B **616**, 25 (2005).
[16] H. S. Lee *et al.*, Phys. Rev. Lett. **99**, 091301 (2007).
[17] G. J. Alner *et al.*, Phys. Lett. B **616**, 17 (2005).
[18] S. Archambault *et al.*, Phys. Lett. B **682**, 185 (2009).
[19] Z. Ahmed *et al.*, Phys. Rev. D **84**, 011102 (2011).
[20] E. Aprile *et al.*, Phys. Rev. Lett. **107**, 131302 (2011).
[21] C. E. Aalseth *et al.*, Phys. Rev. Lett. **107**, 141301 (2011).
[22] G. Angloher *et al.*, arXiv:1109.0702.
[23] Z. Ahmed *et al.*, Science **327**, 1619 (2010).
[24] A. Martin, arXiv:hep-ph/0602206.
[25] A. Birkedal, A. Noble, M. Perelstein, and A. Spray, Phys. Rev. D **74**, 035002 (2006).
[26] G. Bélanger, M. Kakizaki, and A. Pukhov, J. Cosmol. Astropart. Phys. 02 (2011) 009.
[27] U. Ellwanger, C. Hugonie, and A. M. Teixeira, Phys. Rep. **496**, 1 (2010).
[28] G. Bertone, D. G. Cerdeno, M. Fornasa, R. R. de Austri, C. Strege, and R. Trotta, J. Cosmol. Astropart. Phys. 01 (2012) 015.
[29] B. C. Allanach and D. Hooper, J. High Energy Phys. 10 (2008) 071.
[30] O. Buchmueller, R. Cavanaugh, D. Colling, A. De Roeck, M. J. Dolan, J. R. Ellis, H. Flacher, and S. Heinemeyer *et al.*, Eur. Phys. J. C **71**, 1722 (2011).
[31] O. Buchmueller, R. Cavanaugh, D. Colling, A. De Roeck, M. J. Dolan, J. R. Ellis, H. Flacher, and S. Heinemeyer *et al.*, Eur. Phys. J. C **71**, 1583 (2011).
[32] A. Fowlie, A. Kalinowski, M. Kazana, L. Roszkowski, and Y. L. S. Tsai, arXiv:1111.6098.
[33] D. E. Lopez-Fogliani, L. Roszkowski, R. R. de Austri, and T. A. Varley, Phys. Rev. D **80**, 095013 (2009).
[34] H. Baer, E.-K. Park, and X. Tata, New J. Phys. **11**, 105024 (2009).
[35] Y. Akrami, P. Scott, J. Edsjo, J. Conrad, and L. Bergstrom, J. High Energy Phys. 04 (2010) 057.
[36] G. Bélanger, F. Boudjema, A. Cottrant, A. Pukhov, and A. Semenov, Nucl. Phys. **B706**, 411 (2005).
[37] H. Baer, A. Mustafayev, E.-K. Park, and X. Tata, J. High Energy Phys. 05 (2008) 058.
[38] C. F. Berger, J. S. Gainer, J. L. Hewett, and T. G. Rizzo, J. High Energy Phys. 02 (2009) 023.
[39] S. S. AbdusSalam, B. C. Allanach, F. Quevedo, F. Feroz, and M. Hobson, Phys. Rev. D **81**, 095012 (2010).
[40] G. Bélanger, F. Boudjema, A. Pukhov, and R. K. Singh, J. High Energy Phys. 11 (2009) 026.
[41] S. Sekmen, S. Kraml, J. Lykken, F. Moortgat, S. Padhi, L. Pape, M. Pierini, and H. B. Prosper *et al.*, arXiv:1109.5119 [J. High Energy Phys. (to be published)].
[42] A. Arbey, M. Battaglia, and F. Mahmoudi, Eur. Phys. J. C **72**, 1847 (2012).
[43] A. Bottino, F. Donato, N. Fornengo, and S. Scopel, Phys. Rev. D **70**, 015005 (2004).
[44] A. Bottino, F. Donato, N. Fornengo, and P. Salati, Phys. Rev. D **72**, 083518 (2005).
[45] Y. Mambrini, C. Munoz, and E. Nezri, J. Cosmol. Astropart. Phys. 12 (2006) 003.
[46] L. Roszkowski, R. R. de Austri, J. Silk, and R. Trotta, Phys. Lett. B **671**, 10 (2009).
[47] F. Donato, D. Maurin, P. Brun, T. Delahaye, and P. Salati, Phys. Rev. Lett. **102**, 071301 (2009).
[48] P. Scott, J. Conrad, J. Edsjo, L. Bergstrom, C. Farnier, and Y. Akrami, J. Cosmol. Astropart. Phys. 01 (2010) 031.
[49] J. Ellis, K. A. Olive, and V. C. Spanos, J. Cosmol. Astropart. Phys. 10 (2011) 024.
[50] H. Baer, A. Belyaev, T. Krupovnickas, and J. O'Farrill, J. Cosmol. Astropart. Phys. 08 (2004) 005.
[51] A. Bottino, F. Donato, N. Fornengo, and S. Scopel, Phys. Rev. D **77**, 015002 (2008).
[52] L. Bergstrom, T. Bringmann, and J. Edsjo, Phys. Rev. D **83**, 045024 (2011).

[53] G. Bertone, D. G. Cerdeno, M. Fornasa, L. Pieri, R. R. de Austri, and R. Trotta, arXiv:1111.2607 [Phys. Rev. D (to be published)].

[54] D. Albornoz Vásquez, G. Bélanger, C. Boehm, A. Pukhov, and J. Silk, Phys. Rev. D **82**, 115027 (2010).

[55] D. Albornoz Vásquez, G. Bélanger, and C. Boehm, Phys. Rev. D **84**, 095015 (2011).

[56] D. Santos *et al.*, J. Phys. Conf. Ser. **309**, 012014 (2011).

[57] E. Daw, J. R. Fox, J. -L. Gauvreau, C. Ghag, L. J. Harmon, M. Gold, E. Lee, and D. Loomba *et al.*, Astropart. Phys. **35**, 397 (2012).

[58] S. Ahlen *et al.*, Phys. Lett. B **695**, 124 (2011).

[59] S. E. Vahsen *et al.*, in *EAS Publications Series* (Cambridge University Press, Cambridge, England, 2012), Vol. 53, p. 43.

[60] T. Naka *et al.*, in *EAS Publications Series* (Cambridge University Press, Cambridge, England, 2012), Vol. 53, p. 51.

[61] K. Miuchi *et al.*, Phys. Lett. B **686**, 11 (2010).

[62] J. R. Ellis and R. A. Flores, Phys. Lett. B **263**, 259 (1991).

[63] M. S. Alenazi and P. Gondolo, Phys. Rev. D **77**, 043532 (2008).

[64] A. M. Green, J. Cosmol. Astropart. Phys. 10 (2010) 034.

[65] P. D. Serpico and G. Bertone, Phys. Rev. D **82**, 063505 (2010).

[66] F. S. Ling, E. Nezri, E. Athanassoula, and R. Teyssier, J. Cosmol. Astropart. Phys. 02 (2010) 012.

[67] S. H. Hansen and B. Moore, New Astron. Rev. **11**, 333 (2006).

[68] M. C. Smith *et al.*, Mon. Not. R. Astron. Soc. **399**, 1223 (2009).

[69] P. Gondolo, Phys. Rev. D **66**, 103513 (2002).

[70] J. D. Lewin and P. F. Smith, Astropart. Phys. **6**, 87 (1996).

[71] S. Henderson, J. Monroe, and P. Fisher, Phys. Rev. D **78**, 015020 (2008).

[72] M. W. Goodman and E. Witten, Phys. Rev. D **31**, 3059 (1985).

[73] G. Bélanger, E. Nezri, and A. Pukhov, Phys. Rev. D **79**, 015008 (2009).

[74] G. Aad *et al.* (ATLAS Collaboration), arXiv:1109.6572.

[75] D. R. Tovey, R. J. Gaitskell, P. Gondolo, Y. Ramachers, and L. Roszkowski, Phys. Lett. B **488**, 17 (2000).

[76] M. Cannoni, Phys. Rev. D **84**, 095017 (2011).

[77] E. Moulin, F. Mayet, and D. Santos, Phys. Lett. B **614**, 143 (2005).

[78] E. Moulin, Ph.D. thesis, Université Joseph Fourier Grenoble (France), 2005.

[79] F. Giuliani and T. A. Girard, Phys. Rev. D **71**, 123503 (2005).

[80] V. A. Bednyakov and F. Simkovic, Phys. Part. Nucl. **36**, 131 (2005).

[81] P. C. Divari, T. S. Kosmas, J. D. Vergados, and L. D. Skouras, Phys. Rev. C **61**, 054612 (2000).

[82] A. F. Pacheco and D. Strottman, Phys. Rev. D **40**, 2131 (1989).

[83] B. H. Wildenthal, Prog. Part. Nucl. Phys. **11**, 5 (1984).

[84] D. Hooper and T. Plehn, Phys. Lett. B **562**, 18 (2003).

[85] G. Bélanger, F. Boudjema, A. Pukhov, and S. Rosier-Lees, arXiv:hep-ph/0212227.

[86] A. Bottino, N. Fornengo, and S. Scopel, Phys. Rev. D **67**, 063519 (2003).

[87] G. Bélanger, F. Boudjema, A. Cottrant, A. Pukhov, and S. Rosier-Lees, J. High Energy Phys. 03 (2004) 012.

[88] A. Bottino, F. Donato, N. Fornengo, and S. Scopel, Phys. Rev. D **68**, 043506 (2003).

[89] G. Bélanger, F. Boudjema, C. Hugonie, A. Pukhov, and A. Semenov, J. Cosmol. Astropart. Phys. 09 (2005) 001.

[90] G. Bélanger, F. Boudjema, A. Pukhov, and A. Semenov, Comput. Phys. Commun. **180**, 747 (2009).

[91] G. Bélanger, F. Boudjema, P. Brun, A. Pukhov, S. Rosier-Lees, P. Salati, and A. Semenov, Comput. Phys. Commun. **182**, 842 (2011).

[92] G. Bélanger, F. Boudjema, A. Pukhov, and A. Semenov, Comput. Phys. Commun. **177**, 894 (2007).

[93] A. Djouadi, J. -L. Kneur, and G. Moultaka, Comput. Phys. Commun. **176**, 426 (2007).

[94] U. Ellwanger and C. Hugonie, Comput. Phys. Commun. **175**, 290 (2006).

[95] A. Djouadi, M. M. Muhlleitner, and M. Spira, Acta Phys. Pol. B **38**, 635 (2007), http://th-www.if.uj.edu.pl/acta/vol38/abs/v38p0635.htm.

[96] P. Bechtle, O. Brein, S. Heinemeyer, G. Weiglein, and K. E. Williams, Comput. Phys. Commun. **181**, 138 (2010).

[97] P. Bechtle, O. Brein, S. Heinemeyer, G. Weiglein, and K. E. Williams, Comput. Phys. Commun. **182**, 2605 (2011).

[98] S. Chatrchyan *et al.* (CMS Collaboration), Phys. Rev. Lett. **106**, 231801 (2011).

[99] S. Chatrchyan *et al.* (CMS Collaboration), CMS Report No. PAS HIG-11-011.

[100] K. Nakamura *et al.* (Particle Data Group Collaboration), J. Phys. G **37**, 075021 (2010).

[101] D. Albornoz Vásquez, G. Bélanger, and C. Boehm, Phys. Rev. D **84**, 095008 (2011).

[102] A. A. Abdo, M. Ackermann, M. Ajello, W. B. Atwood, L. Baldini, J. Ballet, G. Barbiellini, and D. Bastieri *et al.*, Astrophys. J. **712**, 147 (2010).

[103] D. Albornoz Vásquez, G. Bélanger, R. M. Godbole, and A. Pukhov, arXiv:1112.2200.

[104] E. Komatsu *et al.*, Astrophys. J. Suppl. Ser. **180**, 330 (2009).

[105] J. Giedt, A. W. Thomas, and R. D. Young, Phys. Rev. Lett. **103**, 201802 (2009).

[106] P. Draper, T. Liu, C. E. M. Wagner, L. -T. Wang, and H. Zhang, Phys. Rev. Lett. **106**, 121805 (2011).

[107] K. Griest and D. Seckel, Phys. Rev. D **43**, 3191 (1991).

[108] C. Boehm *et al.* (to be published).

[109] C. McCabe, Phys. Rev. D **82**, 023530 (2010).

[110] M. Kuhlen, N. Weiner, J. Diemand, P. Madau, B. Moore, D. Potter, J. Stadel, and M. Zemp, J. Cosmol. Astropart. Phys. 02 (2010) 030.

[111] P. J. Fox, J. Liu, and N. Weiner, Phys. Rev. D **83**, 103514 (2011).

[112] P. J. Fox, G. D. Kribs, and T. M. P. Tait, Phys. Rev. D **83**, 034007 (2011).

[113] L. E. Strigari and R. Trotta, J. Cosmol. Astropart. Phys. 11 (2009) 019.

[114] D. G. Cerdeno and A. M. Green, in *Particle Dark Matter: Observations, Models and Searches*, edited by G. Bertone (Cambridge University Press, Cambridge, England, 2010), pp. 347-369.

[115] A. M. Green, arXiv:1004.2383.